



**Faculty of Engineering**

**Characterization of Mixing Performance and Droplet Generation in  
Fabricated T-junction and Offset T-junction Microfluidic Devices**

**Hawa Anak Ringkai**

**Master of Engineering  
2021**

Characterization of Mixing Performance and Droplet Generation in  
Fabricated T-junction and Offset T-junction Microfluidic Devices

Hawa Anak Ringkai

A thesis submitted

In fulfillment of the requirements for the degree of Master of Engineering

(Mechanical Engineering)

Faculty of Engineering  
UNIVERSITI MALAYSIA SARAWAK

2021



## **ACKNOWLEDGEMENT**

I would like to express my deepest appreciation to Ir. Dr. Khairul Fikri bin Tamrin, my supervisor for the assistance and helpful guidance throughout this final year project. I am also grateful for the professionalism, compassion and patience shown by him during this period that helped me a lot toward the completion of this project.

My sincere gratitude to the lecturers and friends, especially from the Department of Mechanical and Manufacturing Engineering, Faculty of Engineering UNIMAS, for the continuous advice and support given throughout this project period. This research is fully-supported by the UNIMAS Zamalah Graduate Scholarship (ZSU).

Finally, yet importantly, I would like to pay my highest respect to my family, who keeps giving me positive motivation towards life and challenges, to strengthen me, both physically and mentally.

Thank you.

## ABSTRACT

To date, microfluidic device has contributed significantly in biotechnology and life sciences due to their fast response time, low consumption of samples and high sensitivity. Although it is widely utilized in bio-, nano-, and environmental technologies, there are still limited experimental investigations on the micromixing process of dissimilar liquids. In this study, the mixing process of propan-2-ol and water, water and sodium chloride solution, propan-2-ol and sodium chloride solution were experimented and reported at  $5 \leq Re \leq 50$  in T-junction and offset T-junction microfluidic channel. For miscible mixing experiments, both microchannels show better performance at high Reynolds number of 40 and 50 due to the significant convection which is caused by the effect of stretching and thinning of liquid lamellae. Meanwhile, for immiscible mixture, offset T-junction yielded superior mixing performance than T-junction microchannel at both low and high Reynolds number. Hence, due to the fact that offset T-junction performs better than T-junction, the study was furthered by characterising the behaviours of water-in-oil droplet at interfacial surface within offset T-microchannel having different size i.e., radius of 400  $\mu\text{m}$ , 500  $\mu\text{m}$ , 750  $\mu\text{m}$  and 1000  $\mu\text{m}$  using micro-PIV software. The results showed that experimental velocity of the water droplet holds good agreement with theoretical values, having minimal difference as low as 0.004 mm/s for the case of microchannel with radius 750  $\mu\text{m}$ . A maintained average velocity of 0.000055 m/s for channel with radius of 1000  $\mu\text{m}$  was achieved, meanwhile the other channels showed a good average velocity data i.e., an increase from 0.00015 m/s to 0.0002 m/s for channel radius of 500  $\mu\text{m}$ . In addition, a major elevation for mean velocity from 0.000055 m/s to 0.00015 m/s for channel with radius of 750  $\mu\text{m}$  was also seen.

**Keywords:** microfluidic, micromixing, T-junction, droplet, micro-PIV

***Pencirian Prestasi Pencampuran dan Penghasilan Titisan dalam Fabrikasi Peranti Mikrofluidik Simpang-T dan Pengimbang Simpang-T***

**ABSTRAK**

*Sehingga kini, alat mikrofluidik telah memberikan sumbangan yang besar dalam bioteknologi dan sains kehidupan kerana masa tindak balasnya yang cepat, penggunaan sampel yang rendah dan kepekaan yang tinggi. Walaupun digunakan secara meluas dalam teknologi bio, nano, dan persekitaran, masih ada kajian eksperimental yang terhad mengenai proses pencampuran mikro cecair yang tidak serupa. Dalam kajian ini, proses pencampuran larutan propan-2-ol dan air, air dan natrium klorida, larutan propan-2-ol dan natrium klorida dieksperimen dan dilaporkan pada  $5 \leq Re \leq 50$  dalam saluran mikrofluidik simpang-T dan pengimbang simpang-T. Untuk eksperimen pencampuran cecair yang boleh larut, kedua-dua saluran mikro menunjukkan prestasi pencampuran yang lebih baik pada bilangan Reynolds yang tinggi iaitu 40 dan 50 kerana perolakan yang ketara yang disebabkan oleh kesan regangan dan penipisan lamela cecair. Sementara itu, untuk pencampuran cecair tidak larut, pengimbang simpang-T menghasilkan prestasi pencampuran yang lebih baik daripada saluran mikro simpang-T pada bilangan Reynolds rendah dan tinggi. Oleh itu, disebabkan oleh fakta bahawa pengimbang simpang-T menunjukkan prestasi lebih baik daripada simpang-T, kajian ini dilanjutkan dengan mencirikan kelakuan titisan air dalam minyak pada permukaan antara muka dalam saluran mikro pengimbang simpang-T dengan saiz yang berbeza iaitu, jejari 400  $\mu\text{m}$ , 500  $\mu\text{m}$ , 750  $\mu\text{m}$  dan 1000  $\mu\text{m}$  menggunakan perisian mikro-PIV. Hasil kajian menunjukkan bahawa halaju eksperimen titisan air dalam persamaan dengan nilai teori, dengan perbezaan minimum serendah 0.004 mm/s untuk kes saluran mikro dengan jejari 750  $\mu\text{m}$ . Pengendalian halaju rata-rata sebanyak 0.000055 mm/s untuk saluran jejari 1000  $\mu\text{m}$  dicapai, sementara*

*saluran lain menunjukkan data halaju rata-rata yang baik, iaitu peningkatan dari 0.00015 mm/s ke 0.0002 mm/s untuk saluran jejari 500  $\mu\text{m}$ . Selain itu, peningkatan terbanyak untuk halaju min dari 0.000055 mm/s ke 0.00015 mm/s untuk saluran jejari 750  $\mu\text{m}$  juga terlihat.*

**Kata kunci:** *mikrofluidik, pencampuran mikro, simpang-T, titisan, mikro-PIV*

## TABLE OF CONTENTS

	<b>Page</b>
DECLARATION	i
ACKNOWLEDGEMENT	ii
ABSTRACT	iii
ABSTRAK	iv
TABLE OF CONTENTS	vi
LIST OF TABLES	ix
LIST OF FIGURES	x
LIST OF ABBREVIATIONS	xii
<b>CHAPTER 1 INTRODUCTION</b>	<b>14</b>
1.1 Background Study	14
1.2 Problem Statement	17
1.3 Objectives	19
<b>CHAPTER 2 LITERATURE REVIEW</b>	<b>20</b>
2.1 Overview	20
2.2 General Applications of Microfluidic Device	20
2.3 Microfluidic Device for Micromixing Process	24
2.3.1 Numerical Simulation of Micromixing	25
2.3.2 Experimental Investigation of Micromixing	28

2.3.3	Characterization of Micromixing Performance	31
2.4	Microfluidic Device for Bubble/Droplet Generation	33
2.4.1	Characterization of Droplet Generation by Micro-PIV	34
2.4.2	Parameters Affecting Generated Droplet Behaviours	37
2.5	Conclusion	42
<b>CHAPTER 3 MATERIALS AND METHODS</b>		<b>43</b>
3.1	Overview	43
3.2	Fabrication of Microfluidic Channel	43
3.3	Experimental Setup for Micromixing	46
3.3.1	Micromixing Characterization by RGB Colour Model	48
3.4	Experimental Setup and Micro-PIV Processing for Droplet Generation	49
<b>CHAPTER 4 RESULTS AND DISCUSSION</b>		<b>53</b>
4.1	Overview	53
4.2	Micromixing	53
4.2.1	Effect of Channel's Design on The Mixing Index of Two Dissimilar Miscible Liquids (Propan-2-ol and Water)	53
4.2.2	Effect of Channel's Design on The Mixing Index of Two Dissimilar Miscible Liquids (Water and Sodium Chloride Solution)	57
4.2.3	Effect of Channel's Design on The Mixing Index of Two Dissimilar Immiscible Liquids (Propan-2-ol and Sodium Chloride Solution)	60
4.3	Droplet Generation	64

4.3.1	Evolution of Water Droplets at The Junction of Offset T-microchannel	64
4.3.2	Experimental Velocity of Water Droplets at The Junction of Offset T-channel	66
4.3.3	Internal Velocity Profile of Generated Water Droplets	69
<b>CHAPTER 5 CONCLUSION AND RECOMMENDATIONS</b>		<b>84</b>
5.1	Conclusion	84
5.2	Recommendations	86
<b>REFERENCES</b>		<b>88</b>
<b>APPENDICES</b>		<b>99</b>

## LIST OF TABLES

	<b>Page</b>
Table 3.1: Mixing experiments	47
Table 3.2: Controlled parameters	51
Table 3.3: Specification of seeding particle (Turner et al., 2018)	52
Table 4.1: Theoretical and experimental velocity of water droplets	69

## LIST OF FIGURES

	<b>Page</b>
Figure 3.1: Fabricated (a) T-junction and (b) offset T-junction microchannels with inlets and outlet radius of 750 $\mu\text{m}$ for micromixing experiment	44
Figure 3.2: CO <sub>2</sub> FABOOL Laser Mini	45
Figure 3.3: Fabricated offset T-junction microchannel with inlets and outlet radius of 750 $\mu\text{m}$ for droplet generation experiment	45
Figure 3.4: Experimental setup	47
Figure 3.5: Schematic diagram of the experimental setup for droplet generation	51
Figure 4.1: Mixing index of propan-2-ol and water at (a) T-junction, and (b) offset T-junction	55
Figure 4.2: Top view indicating schematically the interdiffusion layer of miscible propan-2-ol-water micromixing in (a) T-junction and (b) offset T-junction microchannels	56
Figure 4.3: Mixing index of water and sodium chloride solution at (a) T-junction, and (b) offset T-junction	58
Figure 4.4: The schematic diagram mixing of water and sodium chloride solution in (a) T-junction, and (b) offset T-junction microchannels	59
Figure 4.5: Mixing index of propan-2-ol and sodium chloride solution at (a) T-junction, and (b) offset T-junction	61

Figure 4.6: Actual mixing images (1400 $\mu\text{m}$ length and 790 $\mu\text{m}$ width) of blue dye in propan-2-ol and yellow dye in sodium chloride solution within offset T-junction microchannel at Reynolds number of 40. MI stands for mixing index.	63
Figure 4.7: Comparison of mixing index between propan-2-ol and sodium chloride solution at different Reynolds number in T-junction and offset T-junction microchannels	64
Figure 4.8: The evolution of water droplets for offset T-microchannels with radius of (a) 400 $\mu\text{m}$ , and (b) 750 $\mu\text{m}$	66
Figure 4.9: The motion of water droplets after 364 ms within radius of (a) 400 $\mu\text{m}$ , (b) 500 $\mu\text{m}$ , and (c) 750 $\mu\text{m}$ offset T-microchannels	68
Figure 4.10: Internal velocity profile of generated water droplet for offset T-microchannel with radius of 400 $\mu\text{m}$	74
Figure 4.11: Internal velocity profile of generated water droplet for offset T-microchannel with radius of 500 $\mu\text{m}$	77
Figure 4.12: Internal velocity profile of generated water droplet for offset T-microchannel with radius of 750 $\mu\text{m}$	80
Figure 4.13: Internal velocity profile of generated water droplet for offset T-microchannel with radius of 1000 $\mu\text{m}$	83

## LIST OF ABBREVIATIONS

ATCC	American Type Culture Collection
CCD	Charge-coupled device
CFD	Computational Fluid Dynamics
CO <sub>2</sub>	Carbon dioxide
DC	Direct current
H <sub>3</sub> BO <sub>3</sub>	Boric acid
IOS	Intensity of Segregation
KI	Potassium iodide
KIO <sub>3</sub>	Potassium iodate
MATLAB	Matrix laboratory
MEMS	Microelectromechanical system
NaOH	Sodium hydroxide
Nd: YLF	Neodymium-doped yttrium lithium fluoride
NEMA	National Electrical Manufacturers Association
NIH	National Institutes of Health
p-ATP	Paminothiophenol
PDMS	Polydimethylsiloxane
PIV	Particle image velocimetry
PLIF	Planar laser induced fluorescence
PMMA	Poly (methyl methacrylate)
RGB	Red, green, blue
SERS	Surface enhanced Raman scattering

$\mu$ -LIF	Micro-laser induced fluorescence
$\mu$ TAS	Micrototal analysis system

## CHAPTER 1

### INTRODUCTION

#### 1.1 Background Study

Over the years, microfluidic devices have been developed significantly for microelectromechanical system (MEMS), microchemical technology and micrototal analysis system ( $\mu$ TAS). For instance, micromixing process in microfluidic devices has been widely employed in bio-, nano-, and environmental technologies for biomedical and health related issues (Kim & Yoon, 2017; Kumar Mondal & Wongwises, 2020). It also extensively applied in food and chemical industries. Generally, most of the applications either involve use of miscible or immiscible liquids (Fornerod et al., 2020).

The purposes of mixing in microfluidic device are to improve the efficiency of mixing by reducing the characteristics size of microscale devices within shorter mixing channels (Lee et al., 2011) and the cost of laboratory equipment as it diminishes the consumption of specimens (Solehati et al., 2014; Viktorov et al., 2016). Moreover, the aim here is to obtain fast and complete mixing of different samples of fluids in the devices/geometry involving microfluidics. In general, the mixing of the liquid sample species in microfluidic devices under different configurations is majorly dominated by diffusion process (Lee et al., 2011). However, microscale mixing remains a challenge due to the inefficient mixing in microfluidics system (Shah, Su Jeon, et al., 2019) which is primarily governed by slow molecular diffusion (Lee & Fu, 2018) since the mixing time is directly proportional to the square of the channel width over the molecular diffusivity (Aubin et al., 2010).

To better understand the micromixing process, there are a number of numerical studies on the micromixing of different densities and viscosities liquids i.e., water-ethanol mixtures (Jeon et al., 2004; Lin et al., 2007; Wang et al., 2002). Ansari et al. (2010) numerically investigated the mixing performance influenced by the water and ethanol stream interface's positions inside T-junction microchannels at  $0 < Re \leq 10$ . It was found that the interface's position in the channel for low Reynolds number,  $Re < 10$  had a major impact on mixing compared to the ones at higher Reynolds number,  $Re > 10$ . Chung and Shih (2008) used a planar micromixer with rhombic microchannels and a converging-diverging element to study the mixing of ethanol and water, and found that over 90% mixing can be achieved at  $30^\circ$  turning angle and  $Re \geq 200$ . This proved that the rhombic micromixer has potential to be used in the future applications of fast and high throughput mixing. Orsi et al. (2013) performed numerical study on the mixing behaviours of water-ethanol in T-junction microchannel for Reynolds number ranging from 1 to 300 via a commercial Computational Fluid Dynamics (CFD). The numerical data showed a good mixing performance of water-ethanol at  $Re < 100$  due to high viscosity of ethanol and therefore lead to high residence time of the liquids occupying the interfacial region. Meanwhile, at high Reynolds number, water and ethanol streams were separated by a viscous layer led to vortex formation and poor mixing.

Apart from micromixing, the multiphase flow, especially two-phase flow, also occurs so often in the aforementioned microfluidic device applications (Fu et al., 2009). For example, liquid-liquid multiphase flow has numerous applications in mixing process (Günther et al., 2005; J. Wang et al., 2015), chemical reaction (Wu et al., 2019), and also the emulsion technology (Chen et al., 2009; Vladisavljević et al., 2017). One important application of these devices is the generation of monodisperse emulsions and particles that

have precise size and composition (Joensson & Andersson Svahn, 2012; Li et al., 2017; Teh et al., 2008). They rely on the co-axial flow of these immiscible liquids and breaking-up the disperse phase into droplets suspended in the outer continuous liquid with the resulting shear forces through geometric constriction (Shah et al., 2008).

The common geometries used for the microfluidic droplet generation are flow-focusing, co-flow and cross-flow devices. For example, Thurgood et al. (2019) used polydimethylsiloxane (PDMS) based microfluidic flow-focusing channel to investigate the size, gap and generation rate of oil-in-water droplets. They highlighted the ability of asynchronous oil droplet generation with the gap varying from few microns to few hundred microns in successive and rapid cycles. Deng et al. (2018) studied the hydrodynamics of rising droplets i.e., soybean oil and toluene in quiescent water using co-flowing microfluidic device. The results of the experimentations indicated the rigid-sphere like behaviour of single micro-droplet in terms of its terminal velocity; however, the swarm of droplets moves with a higher terminal velocity as compared to a single droplet.

Literally, producing oil-in-water droplets is easier than developing their water-in-oil droplets (Colucci et al., 2020). The real life applications of suspended water droplets is significant such as encapsulating the bioactive compounds for controlled release in fat-based eatable products such as mayonnaise with the purpose of nutrition fortification (Zhu et al., 2019). Other examples in different industrial and environmental applications (Ghannam, 2005) include, crude oil spillage (Sjöblom, 2012), water in heavy crude oil pipeline transportation (Ashrafizadeh & Kamran, 2010), the crude oil extraction mixed with varying proportions of water (Carcoana, 1992), and enhanced oil recovery involving oil-polymer emulsion (Ghannam, 2003). As in droplet based microfluidics experiment, Yao et al. (2019) investigated the effect of different viscosities of carrier oil on water-in-oil emulsion using a

cross-flow device which is T-junction microchannel. The results indicated that with the increase of oil viscosity, the size of droplet decreased and this happened regardless of pressure level of flow.

Micro particle image velocimetry (micro-PIV) method has been widely known technique in the application of microfluidics (Campo-Deaño, 2018; Hagsäter et al., 2007; Omori et al., 2015; Santiago et al., 1998; Shinohara et al., 2004). Moreover, the droplet internal flow details in the microchannels have been characterized mainly by this technique (Hein et al., 2015; Jakiela et al., 2012; Liu et al., 2017; Ma et al., 2014, 2015; Oishi et al., 2011). There are a number of studies involving the use of this method to study the formation of droplets. Liu et al. (2017) studied the internal flow field of water-in-oil droplets traveling in a T-junction microchannel by means of micro-PIV method. One important observation is the impact of the capillary number on the flow physics including its critical value, while geometry of the droplet impacts the axial as well as transverse velocity components. Kinoshita et al. (2007) measured and visualized the internal flow of a moving water/glycerol-in-oil droplet in PDMS T-junction microchannel using confocal micro-PIV system. The measured results revealed that the fluid residing inside the droplet intricately observes a circular three-dimensional motion within the constrained volume as the contacting surfaces, i.e., surrounding walls of the channel, pose drag on the surfaces of the droplet while it moves inside the microchannel. This intricated motion of fluid, within droplet, enhances the mixing and resultantly the chemical reaction in the device, if any.

## **1.2 Problem Statement**

There are limited experimental studies investigating the mixing process between two dissimilar miscible liquids in relation to microfluidics. For example, Lin et al. (2007) experimentally investigated the mixing of ethanol and water using T-junction microchannel

having J-shaped baffle. Due to unequal lateral perturbation, it was found that the mixing performance increases with the increase of baffle number as high convection and molecular redistribution occurred along the main channel. Wang et al. (2012) investigated micromixing of water-water and water-ethanol in T-junction microchannel. Mixing performance of water-ethanol was found better than that of water-water due to the former having dissimilar densities which effectively improved driving force of mass transfer at the interface. To the best of authors' knowledge, there are also limited studies on experimental investigation and characterization of mixing performance of two immiscible liquids.

Meanwhile, in a different study i.e., droplet generation process, Jin and Yoo (2012) conducted flow visualization via micro-PIV to investigate water/glycerol-in-oil droplet merging processes in a main Y-microchannel which is connected downstream to a straight channel or a divergent channel. The results for a straight channel confined droplet suggest that the rear droplets, at the time coalescence, penetrated the front droplets. While in the divergent channel geometry, as the droplet merges a strong vortex motion is generated resulting in the rear droplet enveloping the front droplets. Shen et al. (2017) investigated fundamental flow characteristics of water-ethanol droplet suspended in sunflower oil merging in T-junction channel and rectangular microgroove, and splitting in two different microstructures i.e., cylinder obstruction and Y-junction bifurcation via micro-PIV technique. The microgroove generates higher probability for the coalescence of droplet compared to the T-junction in a microchannel. While, the junction of Y-shape can result in microdroplets splitting with a higher efficiency ( $\eta > 95\%$ ) while keeping the microdroplet flow steady during the splitting at the junction. The existed studies focused on the different shape of the microchannels for droplet merging and splitting process, with less consideration given to the size or diameter of the microchannels (Darekar et al., 2017; Kashid & Agar,

2007; Salim et al., 2008), which also one of the channel geometry's property that can affect the flow characteristics of the droplets.

### **1.3 Objectives**

The main objectives of this research are:

- i. To design and fabricate T-junction and offset T-junction microchannels using electric drill
- ii. To characterize mixing index of dissimilar liquids at  $5 \leq Re \leq 50$  inside T-junction and offset T-junction microchannels
- iii. To investigate the effect of offset T-junction microchannel's size on water-in-oil droplet's behaviours at interfacial surface using micro-PIV technique

## CHAPTER 2

### LITERATURE REVIEW

#### 2.1 Overview

Chapter 2 provides a summary of literature studies related to microfluidic device application, mainly focused on microfluidic mixing and droplets generation processes that had been conducted in the past. The investigation method particularly on experimental study of both processes will be elaborated. The techniques used to characterize the mixing performance, and also the factors that influence the droplet behaviours will be discussed in Section 2.3 and 2.4, respectively.

#### 2.2 General Applications of Microfluidic Device

Microfluidic device is an instrument that deals with fluids at microscale level. This device has contributed significantly and extensively applied in biotechnology and environmental issues as well as in food and chemical industries due to their fast response time, low consumption of samples and high sensitivity. For example, Pang et al. (2015) presented a new integrated microfluidic device for cancer cell separation based on cell size and deformability by combining the microstructure-constricted filtration and pneumatic microvalves system. The problem is aroused when filtration method for cell sorting is always limited by the unpredictable variation of the filter hydrodynamic resistance due to cell accumulation and clogging in the microstructures. Therefore, for each filter unit, they designed two semi-circle and a rectangle, and the two side-by-side units formed a funnel-like shaped to avoid cell damage and enhance the rate of separation. Meanwhile, for the cell separation device, it comprised of filtration constriction arranged in a two-dimensional array with eight group filter matrices for cell capture and sorting, and the membrane microvalves

were used to control the flow across filter matrices. By using this proposed device, the periodical sort and release of cells greatly avoided cell accumulation and clogging and improved the selectivity and successfully separated cancer cells from the blood samples with more than 90% cell recovery and more than 80% purity. To summarize, this microfluidic device provides a new approach for cancer cell separation with high collection recovery and purity.

Kuntaegowdanahalli et al. (2009) studied the principle of Dean-coupled inertial migration in spiral microfluidic device for separating different size of particles. This is because the use of porous membrane filter is not efficient at separating various size particles due to complex fabrication of 3D structures. Standard soft lithography method was used to fabricate five-loop spiral microchannel with two inlets and eight equally spaced outlets. They used polystyrene particles of varying diameters i.e., 10  $\mu\text{m}$ , 15  $\mu\text{m}$  and 20  $\mu\text{m}$ . All these particles come in one mixture. The flow description in the channel is based on Dean number,  $De$  which can be defined as:

$$De = Re \sqrt{\frac{D_h}{2R}} \quad \text{Equation 2.1}$$

where  $Re$  is the Reynolds number,  $D_h$  is the hydraulic diameter of microchannel and  $R$  is the radius of convex surface's curvature.

The microchannel successfully separated all the particles with efficiency of 90%. They further demonstrated the application of their technique for separating neural cells, achieving 80% efficiency.

Wu et al. (2017) proposed a biomimetic artificial cilia-based microfluidic device to address both mixing and propulsion. It is essential to develop a microfluidic device that can

perform multitasking for a wide range of applications. For instance, in drug delivery systems, uniform mixing and propulsion across the depth of the flow domain are necessary. They fabricated a rectangular microfluidic device with four straight microchannels where an array of artificial cilia was embedded within one of the channel's confinement through the microfabrication technique. The experimental results showed that the proposed design had successfully achieved a maximum micromixing efficiency of 84% and flow rate of 0.089  $\mu\text{L}/\text{min}$ . In short, this device can be used as a targeted drug delivery system, where it focuses on a homogeneous mixture between the drug and its carrier prior to its administration into target system.

Ooms et al. (2009) experimented a three-dimensional flow i.e., demineralized water seeded with 2  $\mu\text{m}$  diameter of spherical polystyrene particles in a T-shaped micromixer using digital holographic microscopy to overcome smaller depth-of-field associated with conventional optical microscopy. In this experiment, a Nd: YLF laser with a wavelength of 527 nm and maximum pulse energy of 10 mJ was used. To reduce the deformation of the light beam passing through the T-mixer, high quality glass plates microchannel were used. The system consists of a pressure vessel made of stainless steel and provides constant mass flows to both inlets using two controllers. It can be concluded that digital holographic microscopy is a suitable method to carry out three-dimensional velocity measurements of time independent microscopic flows with sufficient accuracy and spatial resolution. Using high speed multiple frame measurements to record the polystyrene particles in multiple consecutive holograms proved that microscopy could successfully follow the particles in a three-dimensional measurement domain.

Kim and Breuer (2007) introduced the use of bacterial carpets to enhance micromixing in a microfluidic device. This is because it is difficult to find a fluidic actuator

to improve the mixing between parallel streams of fluids. Attachment of flagellated bacteria onto the solid surface can activate a solid-fluid interface, so that the cell and working fluid will be unmixed. In this study, they used 1  $\mu\text{m}$  diameter and 2  $\mu\text{m}$  long of *Serratia marcescens*, a wild American Type Culture Collection (ATCC 274). For microfabrication, soft lithography technique was used to fabricate the fluid devices. The fabricated Y-junction microchannel consisted of two arms, and each arm carried fluid into a main mixing channel having dimension of 28 mm long, 15  $\mu\text{m}$  high and 200  $\mu\text{m}$  wide. At the end of this study, it showed that the bacterial carpets could improve the mixing between two streams in the microchannel. However, due to falling pH, which is affected by high carpet metabolism, the device performance decreased. Thus, bacterial carpet is still unsuitable to replace other conventional technique though it is robust and easy to manufacture.

Xu et al. (2011) presented a flexible integration of high efficiency silver surface enhanced Raman scattering (SERS) monitor in an extended microfluidic device. Previously, the laser-induced fluorescence was used as a high sensitivity optodetection technique but it has some limitations pertaining to detect non-fluorescent product and providing sufficient structural information of the product. In this study, they used a mixture solution of 0.06 M trisodium citrate and 0.08 M silver nitrate aqueous solution. The combination of photolithography and wet-etching technique were used to fabricate the microfluidic channel. An oil immersion objective lens with a numerical aperture of 1.40 and magnification of 100 $\times$ , 800 nm central wavelength of femtosecond laser pulse, two-galvano-mirror set, and Shimadzu spectrometer were used in the experiment. They managed to fabricate microchannel bed of 75  $\mu\text{m}$  wide and 20  $\mu\text{m}$  deep. In the test of paminothiophenol (p-ATP), the detection for SERS signals were chose at three locations, and peak intensity error was not more than 3%, specifying that SERS substrate be in an excellent uniformity. In

conclusion, integrated SERS substrates allows the detection of products in real time during chemical reactions, therefore giving credibility for in situ detection at various positions.

Gelin et al. (2020) experimentally determined the size of oil-in-water droplets by introducing a novel microfluidic device for high-throughput production of monodisperse droplets. This is because low production rate of microfluidic devices remains as one of the major restrictions for their usage in industry. Hence, they developed a three-dimensional emulsifier comprising four nozzles and a magnification of a droplet generator coupled to two inlets i.e., dispersed and continuous phases. From the experimental result, for the four nozzle chips, we show a four folds increase in the production throughput, while maintaining a high monodispersity of the droplets. A scale-up of this proposed device is suitable for industrial applications requiring much larger flow rates than what is typically achievable with microfluidic devices.

### **2.3 Microfluidic Device for Micromixing Process**

Micromixing process in microfluidic devices holds great importance in broad range of industrial applications i.e., biomedical, environmental and chemical industries. The main purpose of mixing in microfluidic device is to improve its percentage performance particular in achieving fast and complete mixing of different samples of fluids by reducing its size i.e., shorter mixing channels and processing cost as it diminishes the consumption of specimens. Hence, in order to have better understanding of micromixing process in microfluidic device, the past studies of the microfluidic mixing by numerical and experimental method done by numerous researchers will be presented in the following sub-sections. The characterization of mixing performance also will be explained in this section.

### 2.3.1 Numerical Simulation of Micromixing

Chen et al. (2016) numerically studied on species mixing performance of micromixers with serpentine microchannels. In order to achieve efficient mixing in a short length channel, the geometry of the micromixer plays dominant role to attain chaotic flow. They developed T-junction microchannels with three different structural design i.e., square-wave, multi-wave and zigzag at 4.7 mm from the junction and analysed their mixing performance for Reynolds number values in the range from 0.1 to 100. The microchannel with square-wave design was found more efficient on mixing compared to the multi-wave and zigzag, especially when Reynolds number is above 100, its mixing efficiency reached beyond 95% with a moderate pressure drop below 50 kPa due to its sharper turns and longer path of the flow. The simulation results demonstrated that the square-wave serpentine micromixer is effective, flexible, and also integrated to a microfluidic system.

Orsi et al. (2013) performed numerical study on the mixing behaviours of two miscible liquids systems i.e., water-water and water-ethanol in T-junction microchannel. There are few previous investigations devoted to study the mixing performance of two dissimilar liquids despite their importance in real microfluidic applications such as pharmaceutical, biomedical and biochemical processes i.e., nano-drugs preparation by antisolvent methods. They carried out the mixing process of two dissimilar miscible liquids systems in microfluidic channel with Reynolds number ranging from 1 to 300 via a commercial Computational Fluid Dynamics (CFD). The numerical data showed the mixing performance of water-ethanol is slightly higher than that of the water-water system at Reynolds number,  $Re < 100$  due to high viscosity of ethanol and therefore lead to high residence time of the liquids occupying the interfacial region. On the contrary, at high

Reynolds number, water and ethanol streams were separated by a viscous layer that led to vortex formation and poor mixing performance.

Wang et al. (2002) enhanced the mixing of water and ethanol by placing obstacles in the Y-microchannel. The problem is aroused because of slow diffusion mixing process caused by laminar flow, and higher pressure drop due to the increase of channel length. In the study, they used theoretical analysis and commercial computational fluid dynamics tool (CoventorWare<sup>TM</sup>) to analyse the mixing performance of the two liquids in a Y-micromixer. The results indicate that asymmetric layout of the obstacle has more effect on the mixing than the number of obstacles. Placing obstacles in the microchannels is a novel method for mixing in microfluidic devices, and the results can provide useful information in the design of these devices.

Ansari et al. (2010) numerically investigated the effect of water and ethanol stream interface's positions inside T-junction microchannels on the mixing index. This is because most of the existing works only focused at one position of the interface of the fluid streams and yet the optimum position where the mixing will be higher in the microchannel is left unknown. Therefore, they conducted a detailed mixing study at different interface positions inside T-junction microfluidic channel for Reynolds number of 0.1, 0.5, 1, 5 and 10. Various position of the interfaces showed significant variations in percentage of mixing at different Reynolds number. It was found that the interface's position in the channel for low Reynolds number,  $Re < 10$  had a major impact on mixing compared to the ones at higher Reynolds number,  $Re > 10$ .

Solehati et al. (2014) enhanced the mixing quality of liquids in a micromixer by proposing T-junction microchannel with wavy structure. This is due to most of the proposed

approaches before added complexities to the design and also manufacturing processes in order to achieve chaotic flow regime at low Reynolds number which can be impractical for some applications. Therefore, they developed two microchannels i.e., straight T-junction and T-junction with wavy structure to compare their mixing index for Reynolds number ranging from 1 to 200. The numerical results showed that T-junction microchannel with wavy structure yields better mixing performance than that of straight T-junction microchannel at higher Reynolds number of 200. This is because the presence of periodically reversed secondary flow generated by curves wavy structure led to chaotic flow regime. The microchannel T-junction with wavy structure can be a desired choice for pharmaceutical industries and chemical processes, where both mixing efficiency and manufacturing process are of huge importance.

Dundi et al. (2019) carried out numerical investigation to enhance liquid mixing at various Reynolds number ( $0 < Re < 750$ ) using T-T microfluidic mixer. This is because the limitations and disadvantages of a simple passive T-junction microchannel found in the past studies i.e., poor mixing at low Reynolds number less than 200 (laminar regime) and high Reynolds number above 400 (pulsating vortex regime). Therefore, they geometrically modified conventional T-junction microfluidic mixer into T-T shaped with each inlet divided into two equal halves with a small gap difference. Mixing performance of T-T microfluidic mixer had shown a remarkable increase for both low and high Reynolds number due to hydrodynamic focusing effect and overlapping of vortices, respectively. In short, T-T shaped passive microchannel is more capable in handling higher throughputs at lower pressure drop, hence it can perform better mixing over a wide range of Reynolds number compared to conventional T-junction micromixer.

### 2.3.2 Experimental Investigation of Micromixing

Shah, Kim, et al. (2019) analysed the effect of Y-junction microfluidic channel with different shape mixing units on mixing performance at  $0 < Re \leq 100$  using experimental method. The problem is aroused because of the difficulty of microchannel with straight shaped design in achieving high mixing efficiency due to molecular diffusion. Therefore, Y-junction with straight channel and another three Y-junction micromixers based on split and recombination principle i.e., Y-shaped circle split and recombination, Y-shaped rhombus-circle split and recombination and Y-shaped rhombus split and recombination were fabricated. It was found that mixing quality of Y-shaped rhombus-circle split and recombination microchannel is much better than the others, especially 99% efficiency at high Reynolds number of 80. The mixing improvement was majorly contributed by mixing units and sharp square bends which led to chaotic advection i.e., rotations and vortices.

Lin et al. (2011) experimentally evaluated the mixing of diluted sulphuric acid and a buffer solution (mixture of  $H_3BO_3$ , NaOH, KI and  $KIO_3$ ) using Y-junction microchannel. The micromixer requirements for microchemical process application differ from the micro total analysis system in aspects of Reynolds number, pressure drop, material and fabrication process. Therefore, they developed stainless steel Y-junction microchannel via the lamination of functional layers with conventional machining and experimented the microchemical liquids under Reynolds number range of 30 to 220. The mixing quality was evaluated based on a parallel-competitive reaction named Villermaux/Dushman reaction by Fournier et al. (1996), where the segregation index of this reaction was considered as the measure of the mixing quality of the micromixer. Improved mixing performance in the main channel can be attributed to its three-dimensional square-wave-shaped and periodic cubic grooves especially at higher flow rate in the range of  $30 \leq Re \leq 220$ .

Wang et al. (2011) experimentally investigate the mixing performance of DI water-glycerol solutions with various viscosities ranging from 0.89 mPa·s to 50.76 mPa·s and total flow rates from 10 ml/h to 140 ml/h in a Y-junction microchannel. The problem is aroused when high mixing yield needs to be achieved for fast mixing liquids especially high viscous liquids with relatively high flow rates. Hence, in this work, they enhanced the micromixing of DI water and glycerol using acoustically induced bubbles at a working frequency range between 0.5 kHz to 3.5 kHz. They achieved 94% mixing performance at viscosity of 5.69 mPa·s between 1 kHz and 2.5 kHz while 78% at high viscosity of 44.75 mPa·s with driving frequency range reduced to 1.5 kHz – 2kHz. Poor mixing is observed for the solutions with the viscosity above 44.75 mPa·s under the entire range of working frequency due to no bubbles inside the microchannel. The mixing enhancement is achieved through the interactions between the oscillating bubbles, acoustic actuation field and the liquids.

Dambrine et al. (2009) studied two dissimilar liquids having different viscosities in a Y-shaped microchannel with outlet dimension twice the size of inlets. This is because a comprehensive description is necessary to evaluate the mixing and interdiffusion process quantitatively. In the study, they used water and water/glycerol as working liquids and measured cartographies of the concentration in glycerol for different flow rates with a Raman confocal microscope equipped with an argon-ion laser. The outcome showed that the interdiffusion layer is not positioned at the center of the microchannel, and its average position evolved towards the transverse direction of the channel geometry during the mixing process. The displacement of the interdiffusion zone was affected by the conservation of the flow rate and of the concentration.

Wang et al. (2012) investigated the micro-mixing process in miscible liquids where two types of representative systems are considered, i.e., water-water (W-W) and water-

ethanol (W-E) using micro-Laser induced fluorescence ( $\mu$ -LIF) technique. This is because the anti-solvent methods always involves both aqueous and organic solutions, which complicates the actual nano-drugs preparation in the pharmaceutical process. The mixing behaviour between these two mixing processes were observed under laminar flow conditions, ranging from 0.5 to 350 Re numbers. The result showed that mixing performance of water-ethanol is better than the water-water mixing due to the distinguished concentration difference between two liquid streams as the effective driving force of mass transfer at the interface. However, the two systems showed similar mixing performance with increasing Re numbers because of enhanced convection. They further the study by demonstrating the nano-drugs preparation using anti-solvent precipitation process. As a result, smaller curcumin nano-precipitation can be achieved at both low and high Re numbers than at medium Re numbers in the microchannel. This corresponds well with the measured mixing performance in the miscible water-ethanol system.

Lin et al. (2007) investigated mixing of ethanol and water in T-junction microchannel having J-shaped baffles using image processing software (NIH Image J). This is due to the unsatisfactory T-junction microchannel's mixing performance found in the literatures. The mixing performances were obtained from the concentrations of the black ink in the fluid along the axial distance that were captured by a CCD camera (DP70, Olympus, Japan) attached to an optical microscope (BX60, Olympus, Japan). The enhanced mixing was observed at the entrance of the main channel having J-shaped baffle that causes unequal lateral perturbation which increases the convection and molecular redistribution along the main channel. It was found the mixing increases with the increase of baffle number and Reynolds number.

Chung and Shih (2008) experimented mixing of ethanol and water using a planar micromixer with rhombic microchannels and a converging-diverging element. The problem is aroused because of the importance of turning angle for varies recirculation area which had not been discussed in their reference. The mixing efficiency was evaluated using image grey level, obtained from the concentration of deep blue ink dye that added to the ethanol for flow visualization. Result indicated that over 90% mixing can be achieved at 30° turning angle and  $Re \geq 200$ . This proved that the rhombic micromixer has potential to be used in the future applications of fast and high throughput mixing.

Ansari et al. (2018) experimentally investigated the mixing performance of water-water in simple and vortex T-junction microchannels at Reynolds number ranging from 1 to 80. This is because a design modification of a simple T-junction microchannel need to be modified for an early development of the mixing which induces complex flow at lower Reynolds number. Hence, they fabricated microfluidic T-junction channel with non-aligned inlet channels, and compared its mixing efficiency to the conventional design of T-channel. The experimental data showed that the mixing efficiency of liquids in the vortex T-junction micromixer is higher than in the conventional simple T-mixer, and is increasing with an increase Reynolds number. This vortex T-junction microfluidic channel is a promising design to efficiently increase mixing and can be applied to all type of micromixers.

### **2.3.3 Characterization of Micromixing Performance**

Fu et al. (2017) improved the reliability of the estimated mixing performance by proposing mixing indexes that consider mean information and dispersion information. This is because the calculation of the quantitative mixing index only utilizes the information of dispersion from the intensity images which give very limited data due to the change in the average intensity with the mixing improvement. They used two practical criteria i.e.,

reliability and repeatability precision to measure the efficiency of the quantitative mixing indexes. According to the comparisons, the proposed method can ensure the reliability of the calculated result every single time and the repeatability precision was less than  $\pm 3.5\%$ . Hence, it can be summarized that mixing indexes considering the combination of mean and dispersion information can provide more reliably results of the mixing performance than the existing mixing indexes methods.

Aubin et al. (2010) analysed the existing experimental techniques used for characterizing mixing and the related phenomena in both single and multiphase flow. The efficiency of mixing in microfluidic devices i.e., chemical reaction, homogenisation, dispersion and emulsification holds a great significance as it will affect several process parameters such as process operating time, mass transfer rates as well as the product quality. Therefore, it is essential to learn and understand the mixing process in micromixers and be able to characterise and evaluate its mixing performance. In the case of single-phase liquid mixing, the mixing performance can be characterized by dilution-based method, either qualitatively using intensity of segregation or the homogeneity of concentration, or quantitatively where mixing time is deduced by determining the length required for visually-complete mixing. Meanwhile, for the case of multiphase liquid-liquid mixing, dilution- and reaction-based method is used by monitoring the dilution of the organic dyes within the mixture and its mixing time can be determined from the grey scale levels in the images.

Zhang et al. (2019) experimentally investigated the effect of Rhodamine 6G and water flow regime on the mixing performance in the T-junction reactor using intensity of segregation (IOS) calculated by grey values via planar laser induced fluorescence (PLIF). The problem is aroused when there is some difference of mixing degree among the simulation works. In the study, they were focusing on the steady and unsteady engulfment

flow at Reynolds number between 50 and 560 to enhance the mixing performance due to increasing interface area of two streams. Result shows that steady engulfment flow at low Reynolds number improved mixing efficiency. On the other hand, unsteady engulfment flow occurred at  $190 < Re < 380$  as the merged vortex passed through the channel and caused periodic oscillation in the chamber. The result of the large eddy simulation shows that the oscillation of vortex merging in the unsteady engulfment flow regime significantly enhance the mixing quality.

Mahmud and Tamrin (2020) improved the mixing index of water-water system in T-junction and Y-junction microchannels at various Reynolds number ranging from 5 to 100 by proposing new RGB colour model technique. The existing studies are mainly based on dispersion (homogeneity) information of the intensity images which individual RGB values are first averaged before mixing index is quantified that can lead to over or underestimate of the calculated mixing index. Hence, by using a new method, they decoded each of the liquids present in the microfluidics according to their respective red R, green G and blue B, and accordingly used to compute the mixing index. The result showed that T-junction microchannel has a slightly better mixing efficiency of 35% than that of Y-junction microchannel with 27.8% efficiency. In short, this RGB colour model method is robust, reliable and foreseen handy in characterizing mixing in real time for gradient mixing in microfluidic devices.

#### **2.4 Microfluidic Device for Bubble/Droplet Generation**

Apart from micromixing process, the other important application of microfluidic devices is the generation of droplet that has precise composition and size. This droplet formation occurs so often in microelectromechanical system (MEMS), microchemical technology, micrototal analysis system ( $\mu$ TAS) as well as in biotechnology applications.

Therefore, to date, there are number of researchers experimentally conducted the bubble/droplet generation in microfluidic device via micro-PIV technique, which their studies will be presented in the next sub-section. The parameters i.e., viscosity, flow rate, interfacial tension, and diameter as well as the wall of the microfluidic channel that affecting the droplet behaviour will be discussed further in this section.

#### **2.4.1 Characterization of Droplet Generation by Micro-PIV**

Shen et al. (2017) investigated fundamental flow characteristics of water-ethanol droplet suspended in sunflower oil in T-junction with rectangular microgroove microchannel via micro-PIV technique. In order to understand the fluid dynamic characteristics of microdroplet merging and splitting processes, a systematic quantitative study is required since the existing studies only focused on the qualitative visualization. They first used two sets of a combination of T-junction and rectangular microgroove in the droplet merging process, and later by the end of the channels, they induced the splitting process of microdroplets in two different microstructures i.e., cylinder obstruction and Y-junction bifurcation, respectively. Based on the results, for droplet merging, the microgroove has a higher microdroplets coalescence efficiency of 92% compared to 50% of that in a T-junction. On the contrary, Y-junction bifurcation can split microdroplets with high efficiency beyond 95% and steadily maintain the microdroplet flow during the break-up process.

X. Wang et al. (2015) measured the internal flow field inside droplet during its formation process influenced by mass transfer using micro-PIV technique. There are few studies concerning mass transfer in droplet generation process, eventhough knowing there is a strong impact between the droplet's internal flow behaviour and the transfer process of the solute i.e., changes in interfacial properties of fluids. They used water as dispersed phase and butanol as continuous phase and experimented both working fluid in a fabricated cross-

flow T-junction microchannel. The results indicated that both size and generation time of droplet decreased as the mass transfer rate increased due to the presence of internal circulation within the droplet during the formation process. The velocity of vortex inside the droplet can be reduced by increasing its mass transfer rate. In short, this experimental result can help to explore the mass transfer mechanism in micro-devices.

Oishi et al. (2011) measured the internal and surrounding flows of a moving droplet in a microfluidic device by developing a multicolour confocal micro-PIV system that features a wavelength separation optical device. This is due to the conventional micro-PIV could not observe the interaction between two liquid phases because it was not purposely designed for multiple phases measurement in which the system cannot separate the tracer images of different phases. In the study, silicone oil as the continuous oil phase and a mixture of dilute water and glycerol as dispersed water phase were used as working liquids and were experimented in a PDMS-based T-junction microchannel. The experimental results successfully clarified the three-dimensional flow structure of each phase and the interaction between the interfaces. As conclusion, the multicolour confocal micro-PIV system also can be applied to chemical reacting flow and high shear flow applications because of the flexibility in the frame rate of the multi-camera system.

Kinoshita et al. (2007) measured and visualized the internal flow of a moving water/glycerol-in-oil droplet in PDMS T-junction microchannel using confocal micro-PIV system. Although micro-PIV is already known as a powerful flow analysis tool to measure velocity profile in a microchannel, it still not competent enough to investigate three-dimensional flow field i.e., internal flow of a droplet, due to its spatial resolution in the vertical direction and acquisition of the out-of-plane velocity component. Hence, they constructed a confocal micro-PIV system using a high-speed scanner and a simple Poiseuille

flow and then applied it to the internal flow of a moving microdroplet. The out-of-focus light was successfully removed and sharp high-contrast particle images were obtained within a thin layer of a horizontal cross-sectional plane which was able to measure velocity distributions of micro-flows in a  $228 \mu\text{m} \times 171 \mu\text{m}$  region with a confocal depth of  $1.88 \mu\text{m}$ . The measurement results indicate that liquid inside a moving droplet circulates intricately and three-dimensionally in a closed channel due to the drag force on the contact surfaces with the surrounding walls of the microchannel. This internal flow phenomenon of a water/glycerol droplet enhances mixing performance and accelerates any chemical reaction in the microfluidic device.

Jin and Yoo (2012) conducted flow visualization via micro-PIV to investigate water/glycerol-in-oil droplet merging processes in a main Y-microchannel which is connected downstream to a straight channel or a divergent channel. The problem is aroused due to few researchers did qualitative visualization studies on the generation of micron-sized droplet in microfluidic channel, yet no one studied and visualized the flow phenomenon during droplet-merging process quantitatively. Thus, they experimentally visualized the water/glycerol droplet-merging in oil inside two different Y-junction with straight and divergent microchannels. Based on the instantaneous velocity vector fields in the dispersed phase during the merging process data, the droplets in the straight channel are confined by the channel walls and the rear droplet penetrates the front droplet at the instant of coalescence. On the contrary, in the divergent channel, a strong vortex motion occurs while the rear droplet envelops the front one.

Liu et al. (2019) experimentally studied the internal flow field of droplets in a curved microchannel using a micro-PIV system. Compared to the straight channel, the internal flow characteristics of the droplet in the curved channel has less cognition despite its significance

for microfluidic flow cytometry i.e., nanocrystal synthesis and cell manipulation applications. Therefore, they experimented glycerine aqueous solution (dispersed phase) and sunflower oil-hexadecane (continuous phase) in a T-junction channel with a bending unit at the outlet. With capillary number varying from  $10^{-3}$  to  $10^{-2}$ , thicker oil film below droplets and its higher velocity across water/oil interface led to the transition from four eddies to three eddies inside droplets, and this similar pattern was also found in the scenario of decrease in viscosity ratio, size of the droplet and channel curvature. When the size of the droplet continuously decreased, the internal eddies inside droplets gradually approached and merged due to a smaller contact area between droplets and oil film. Moreover, surfactants can be added to enhance the reaction performance in fast mixing such as blood, detection of urine sugar and protein synthesis.

#### **2.4.2 Parameters Affecting Generated Droplet Behaviours**

Zhu et al. (2016) quantitatively characterized the formation of glycerol/water droplets in oil phase using a co-flow microchannel with mechanical vibration. The previous researchers successfully demonstrated the capability of mechanical vibration in controlling the droplet break-up process, however a comprehensive and quantitative study concerning the effects of vibration amplitude and frequency, fluid pressure and flow rate on droplet generation remains limited. They modulated a wide range of droplet's size in synchronization region, where the frequency of the droplet generation was synchronized with the vibration frequency, and characterized the maximum synchronization frequency and minimum droplet's size by approximating the fluctuating flow rate of glycerol/water phase. From the experimental results, it was found that the vibration is able to delay the jet formation and allow the dripping to occur in a wider range of flow rates. To summarize, vibration-modulated droplet generation in both dripping and jetting regimes has the

capability to control droplet generation in a more efficient and precise manner for practical applications.

Li et al. (2017) presented new open-channel microfluidic devices based on surfaces with patterned wettability that are competent for water-in-oil emulsification. This is because existing studies related to droplet generation in open channel microfluidic devices were very limited due to the high flow rates requirement to maintain a stable emulsification interface within the channel. The proposed open-channel device capability was enabled by the localized incorporation of different surfaces with selective wettability, including superomniphobic surfaces, and surfaces that are simultaneously hydrophobic and oleophilic. The hydrophobic and oleophilic side walls and the open channels floor greatly improved the flow rate of continuous organic phase, in which enabled the emulsification of the aqueous phase, and prevented this dispersed phase from pinning on different areas of the microchannel. This work represents a continuation of the capability of low-cost open channel microfluidic devices to fabricate hydrophilic microparticles for drug delivery, and potentially the encapsulation of cells within different polymers, both of which are highly desirable within the biological and biomedical fields.

Pang et al. (2014) studied the effect of microchannel's softness on the process of water-in-oil droplet formation for multiphase flows in a T-junction microfluidic device. The soft wall in a microchannel can greatly affect the break-up mechanism of the droplet, as the measured liquid flow rate in the deformed channel is higher than the ones in a non-deforming channel at a given pressure difference. Therefore, they fabricated a new T-junction microchannel with one side of it has a thin PDMS layer that formed a flexible soft wall in which vibrates naturally while droplets are formed. Due to its flexible wall, when the droplets formed, the stresses at the liquid-liquid interface were reduced temporarily as compared to

the case of drop formation in a confined rigid channel. As a consequence, the soft wall reduces the polydispersity in the droplet size. It is believed that this design consideration might be useful in many areas utilizing droplet microfluidics.

Thurgood et al. (2019) used polydimethylsiloxane (PDMS) based microfluidic flow-focusing channel to investigate the size, gap and generation rate of oil-in-water and water-in-oil droplets. This is due to the influence of microfluidic structure's surface properties i.e., hydrophobicity of PDMS on the generation of stable droplets. They reversibly modified the droplet generation characteristics by exposing the channel to water for 48 hours and simply dried the channel with air for a long period. Generation of oil droplets in water occurred as a result of long-term exposure to water while the water-in-oil droplets production caused by the latter. They were able to demonstrate the ability to generate the oil and also water droplets asynchronously and vary the gap between the successive droplets from a few hundred microns to a few microns in successive and rapid cycles.

Yao et al. (2019) investigated the effect of different viscosities of carrier oil on water-in-oil emulsion using a cross-flow device which is T-junction microchannel. Viscosity of the continuous phase is one of the dominant parameters affecting generation rate of droplets since it is highly related to capillary number that influence the break-up of droplet mechanism, yet not many researchers studied its effect in detail. Mineral oil having various viscosities i.e., 4.3 mPa·s, 6.0 mPa·s, 8.6 mPa·s and 12.9 mPa·s respectively was used as a continuous phase while water as the dispersed phase were tested in the microchannel. Due to high linear correlation of droplet generation rate and oil viscosity ( $R^2 = 0.9979$ ) at ratio 3:4 of flow pressure between water and oil, this flow pressure parameter was set constant for all the experiments. The results showed that regardless of the flow pressure levels, the droplet size and droplet generation rate decreased as the oil viscosity increased.

Fu et al. (2009) experimentally investigated the gas bubble formation and break-up process in a microfluidic flow-focusing device at different flow rates for both phases and viscosity for continuous phase using a high-speed digital camera and a micro-PIV technique. The size and geometry of microfluidic devices, flow rates and the fluid properties clearly control the bubble behaviours and their velocity, where their formation process happened very fast that even micro-PIV system having a slightly difficulty to quantify the features of the gaseous thread. They generated the gas bubbles in glycerol-water mixtures inside a  $600\ \mu\text{m} \times 600\ \mu\text{m}$  PMMA square microchannel. Based on the results, bubble break-up process is mostly controlled by the collapse stage, where the collapse rate of the thread neck and the collapse time were influenced by the gas and liquid flow rates as well as the viscosity of the continuous liquid phase. It can be concluded that the elongation and shear stress have a major contribution to the thread break-up in microfluidic devices rather than the capillary instability.

Liu et al. (2017) analysed the internal flow field of water-in-oil droplets inside a cross flow i.e., T-junction microchannel that mainly affected by viscosity ratio using micro-PIV method. It is important to study the factors such as capillary number, viscosity ratio and interfacial tension that led to complex flow patterns, which not much considered and focused by most of the researchers. Therefore, they conducted four experiments using different weightage ratio of dispersed phase (deionized water and glycerol aqueous mixture) that resulted to viscosity ratio and interfacial tension difference between dispersed phase and continuous oil phase. The result showed that larger viscous dissipation led to the formation of additional circulations at a larger capillary number range inside the more viscous droplets compared with the less viscous ones. Two critical capillary numbers were found increased from  $3.2 \times 10^{-3}$  to  $1.9 \times 10^{-2}$  and  $3.8 \times 10^{-2}$  to  $5.0 \times 10^{-2}$  with viscosity ratio varying from

0.018 to 0.220. It was found that the flow pattern heavily relies on capillary number, and geometry of the droplet only affects axial and transverse velocity components values other than the flow behaviours within intervals separated by the critical capillary numbers.

Darekar et al. (2017) analysed the effects of diameter, flow rate, interfacial tension and hydrophobicity of channel wall on the liquid-liquid multiphase flow patterns formed in Y-junction microchannels. The physical property such as the geometry of the microfluidic junction and microchannel has numerous impacts on the flow behaviours, and it is usually difficult to extend the results of a particular combination of the test system and microchannel geometry to a different combination of the test system and microchannel geometry. Therefore, microchannels of two different diameters i.e., 260  $\mu\text{m}$  and 760  $\mu\text{m}$ , with and without hydrophobic coating for each channel were fabricated and used for water droplets in continuous organic phase i.e., butanol, butyl acetate and toluene experiments. Slug flow was found at low flow rates of dispersed and continuous phases, and it changed to slug and droplet flow and then to droplet flow when continuous phase's flow rate was increased at a constant low flow rate of dispersed phase, while changed to parallel flow when dispersed phase's flow rate was increased at a fixed low value of continuous phase's flow rate. As microchannel diameter was reduced, flow pattern transitions were observed to occur at lower flow rates. With increase in interfacial tension, slug flow, slug and droplet flow, and droplet flow became more prominent. Similarly, with hydrophobic coating reduced wetting of the wall by the dispersed phase, slug flow and other dispersed flow pattern became more prominent at the cost of parallel flow.

Deng et al. (2018) studied the hydrodynamics of rising droplets i.e., soybean oil and toluene in quiescent water using co-flowing microfluidic device with various inner and outer diameter that affect the size of the droplet. The problem is aroused due to limitation of

conventional preparation methods lead to lack of experimental data about dynamic behaviours i.e., terminal velocities of micron-sized droplets moving in water. Monodisperse microdroplets with controllable size ranging from 100  $\mu\text{m}$  to 600  $\mu\text{m}$  in co-flowing microchannels were prepared using soybean oil and toluene as dispersed phases and water as the continuous phase. For the same size droplet, the terminal velocity of toluene droplets is higher than the soybean oil droplets since they have greater buoyance force due to their smaller density of  $864.2 \text{ kg/m}^3$  compared to  $917.5 \text{ kg/m}^3$  oil droplets. Their terminal velocity increased linearly with the increasing droplet diameter. The experimental results also show that the terminal velocity of a single microdroplet is consistent with that of calculated rigid spherical particles with the same size and density, while the terminal velocity of a droplet swarm is obviously higher than that of a single droplet.

## **2.5 Conclusion**

In summary, there are two significant usage of microfluidic devices in this research work, which are micromixing process and droplet generation. The applications of both processes have been presented in relevant section of this chapter. The micromixing process application covers both numerical and experimental of the existing studies. All the techniques used to characterize the mixing performance have their own pros and cons, which have been discussed in the above section. The droplet generation past studies including the experimentation via micro-PIV technique and the factors that influence the droplet behaviours have been highlighted as well in this chapter.

## CHAPTER 3

### MATERIALS AND METHODS

#### 3.1 Overview

This chapter focuses on the methodology adopted to conduct micromixing and droplet generation experiments. It covers the microchannel fabrication, experimental setup and also the method used to characterize mixing performance of dissimilar liquids and droplet generation in T-junction microfluidic channel.

#### 3.2 Fabrication of Microfluidic Channel

The first iteration of the fabricated T-junction microchannel consists of a laminated film with average thickness of 250  $\mu\text{m}$  that was sandwiched between poly (methyl methacrylate) (PMMA) sheet and another laminated film with double-sided adhesive sheets. However, propan-2-ol dissolved the adhesive from the double-sided adhesive sheets and cause leakage in the fabricated microchannel.

Figure 3.1 shows the final version of the fabricated T-junction and offset T-junction microchannels for micromixing experiment. Two units of PMMA with thickness of 8 mm were cut using a CO<sub>2</sub> laser (Figure 3.2) to produce microchannel with an overall dimension of 17 mm length and 20 mm width. To remove dust, all the layers were cleaned using clean-room tissue. Then, the PMMA were drilled using drill press machine to form the microchannel shape with inlets and outlet radius of 750  $\mu\text{m}$  and finally, the top end of the outlet port was sealed flushed with the wall using epoxy to avoid the liquids overflow to the top.

The fabricated offset T-junction microchannel for droplet generation experiment is shown in Figure 3.3. The experiment used four units of laser-cut PMMA having overall dimension of 20 mm length, 25 mm width and 6 mm thick. The sheets were drilled using electric mini drill to form offset T-junction microchannel shape with inlets and outlet radius of 400  $\mu\text{m}$ , 500  $\mu\text{m}$ , 750  $\mu\text{m}$  and 1000  $\mu\text{m}$ .

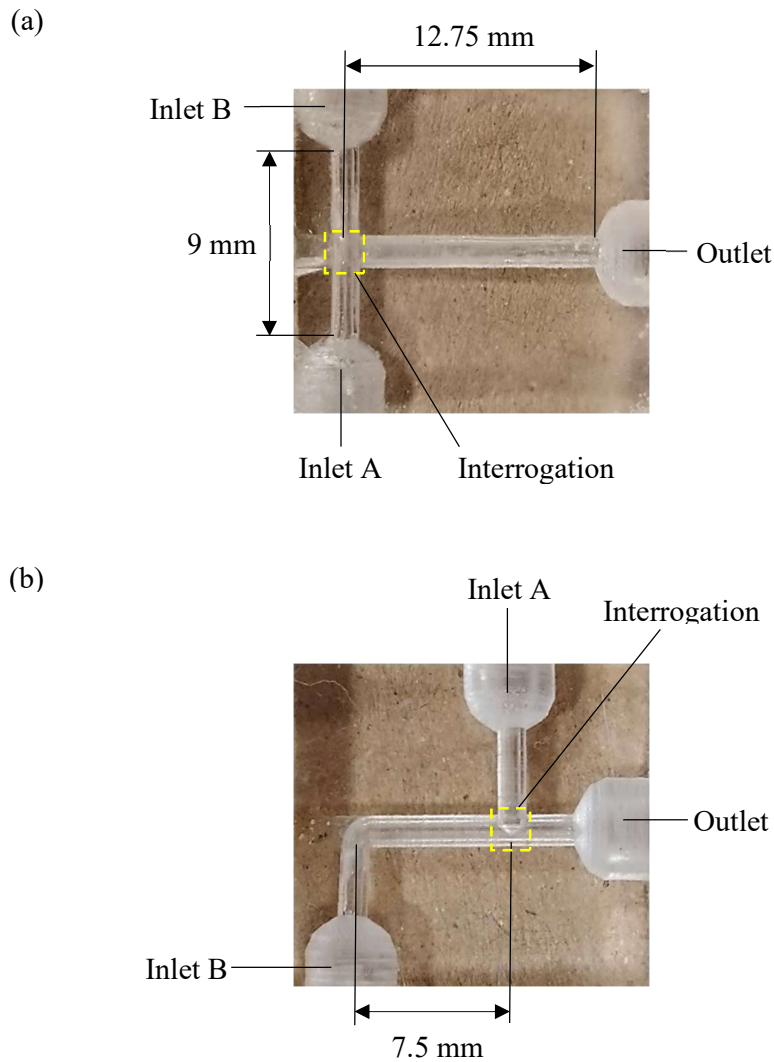


Figure 3.1: Fabricated (a) T-junction and (b) offset T-junction microchannels with inlets and outlet radius of 750  $\mu\text{m}$  for micromixing experiment



Figure 3.2: CO<sub>2</sub> FABOOL Laser Mini

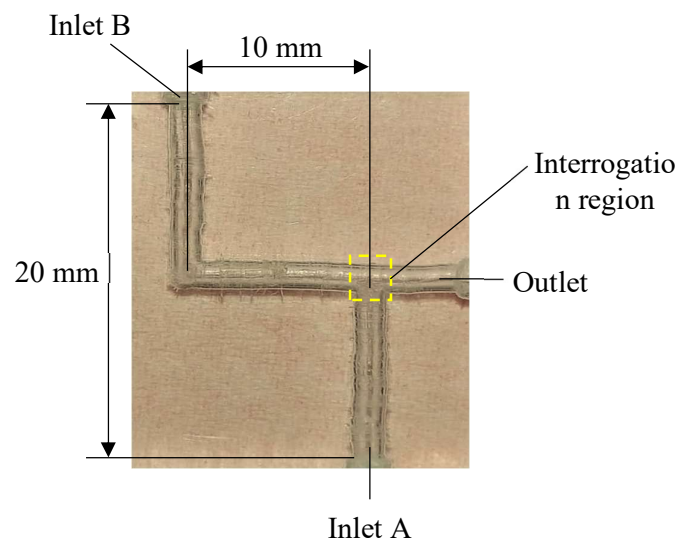


Figure 3.3: Fabricated offset T-junction microchannel with inlets and outlet radius of 750  $\mu\text{m}$  for droplet generation experiment

### 3.3 Experimental Setup for Micromixing

Figure 3.4 shows an experimental setup comprising of fluid driving mechanism, a microfluidic channel and optical imaging system. Both syringes containing dissimilar liquids of coloured solutions with a nominal capacity of 10 mL and volumetric tolerance amounts to  $\pm 4\%$  at room temperature are connected to a lead screw actuated by a two-phase stepper motor (NEMA 17). The stepper motor is controlled by Arduino Uno microcontroller and powered by linear DC power supply (Model: GPS-3030D, Good Will Instrument Co., Ltd). These syringe pump as well as microcontroller and electronic hardware were developed by Mahmud and Tamrin (2020). The resolution of the stepper motor used for the experimentation was increased from 150 to 1800 steps per rotation using A4988 motor driver. The mixing images in microfluidic channel were captured using a digital video microscope (Model: MD500, AmScope) having resolution of  $1280 \times 720$  pixels and  $4\times$  magnification. The whole measurements and experiments were carried out at room temperature  $25 \pm 1$  °C under atmospheric pressure. The settings of the ambient lighting and microscope were also kept constant. Using MATLAB code, the mixing index is quantified using image processing.

The liquids that were injected into inlet A and inlet B for three different mixing experiments were shown in Table 3.1. To quantify the mixing efficiency, blue and yellow food grade dyes were diluted into different liquids with ratio of 1:100 for each mixing experiment. The food dye solution used for the experiment was assumed to have the same density and dynamic viscosity as of water (Mahmud & Tamrin, 2020; Viktorov et al., 2016).

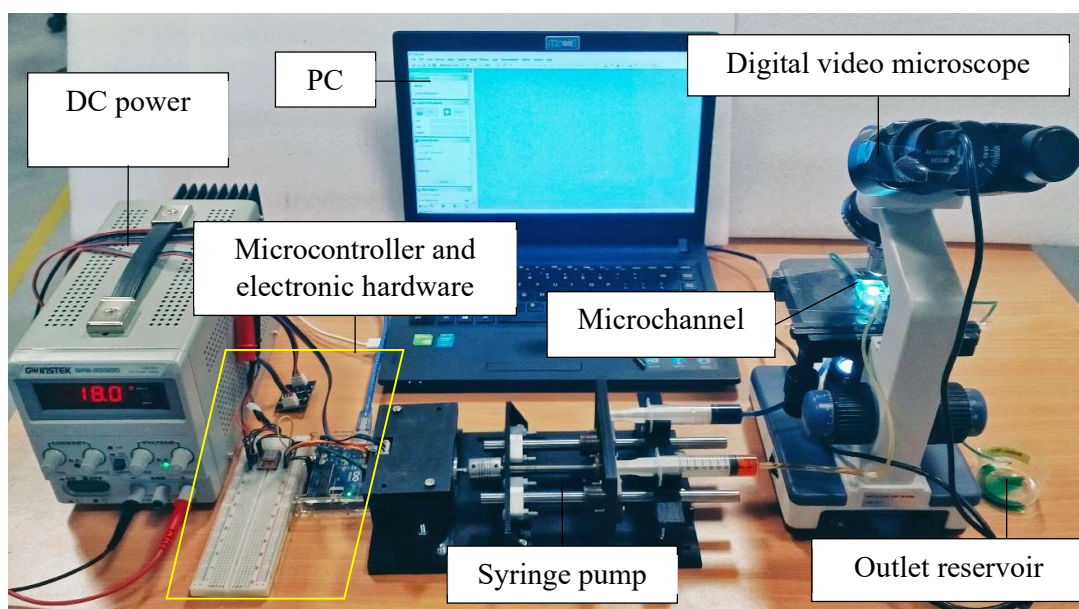


Figure 3.4: Experimental setup

Table 3.1: Mixing experiments

Exp.	Inlet A	Inlet B	Miscibility	Industrial applications
1	Propan-2-ol + blue dye	Water + yellow dye	Miscible	Solvents for cosmetics, antiseptic and cleaning solutions in chemical and pharmaceutical industries.
2	Water + yellow dye	Sodium chloride solution + blue dye	Miscible	Creates saline solution, which can be useful in medical treatment (Nagata, 2018) i.e., cleaning wounds, and also in construction i.e., mixing and curing on the strength of concrete (Giasuddin et al., 2013).
3	Propan-2-ol + blue dye	Sodium chloride solution + yellow dye	Immiscible	The mixture salting out process is useful for production of clean and renewable biofuels (Li et al., 2019), results in the separation of the alcohol from the mixture and formation of a two-phase

				system (Heydari & Mousavi, 2016; Xie et al., 2016).
--	--	--	--	---

Since during the processes of mixing, the density as well as viscosity of the mixture were different, the properties of water were taken as the reference for the whole experiments (Wang et al., 2012) to calculate the flow rate, motor step for the syringe pump's operation and evaluation of mixing performances. The flow rate ( $\text{m}^3/\text{s}$ ) is defined as:

$$Q = \frac{Re \times \mu \times A}{\rho \times D} \quad \text{Equation 3.1}$$

where  $Re$  is Reynolds number (5, 10, 20, 30, 40, 50),  $\mu$  is the dynamic viscosity of water ( $8.9 \times 10^{-4} \text{ Pa}\cdot\text{s}$ ),  $A$  is area of channel ( $1.8 \times 10^{-6} \text{ m}^2$ ),  $\rho$  is the density of water ( $997 \text{ kg/m}^3$ ) and  $D$  is the diameter of the channel ( $1.5 \times 10^{-3} \text{ m}$ ).

### 3.3.1 Micromixing Characterization by RGB Colour Model

Generally, the image intensity is used to find the mixing performance based on the dispersion/homogeneity (Chen et al., 2016; Fu et al., 2017), however such an estimate can result in over and/or under estimate of the mixing index (Mahmud & Tamrin, 2020). For this reason, here the optical method used the RGB colour by decoding each of the mixing images in which the respective intensities in red, green and blue colour pixels can be found using the following equation (Mahmud & Tamrin, 2020):

$$\text{Mixing Index} = \frac{N_{mixed}}{N_{mixed} + N_{unmixed}} \quad \text{Equation 3.2}$$

where  $N_{mixed}$  and  $N_{unmixed}$  are the number of pixels classified as mixed and unmixed solution, respectively, based on the following:

$$N_{mixed} = n(\{r_{g,min} \leq R \leq r_{g,max} \cap g_{g,min} \leq G \leq g_{g,max} \cap b_{g,min} \leq B \leq b_{g,max}\})$$

Equation 3.3

and

$$N_{unmixed} = n(\{r_{b,min} \leq R \leq r_{b,max} \cap g_{b,min} \leq G \leq g_{b,max} \cap b_{b,min} \leq B \leq b_{b,max}\}) + n(\{r_{y,min} \leq R \leq r_{y,max} \cap g_{y,min} \leq G \leq g_{y,max} \cap b_{y,min} \leq B \leq b_{y,max}\})$$

Equation 3.4

here the number of pixels, satisfying RGB conditions, is specified using  $n$  while  $\cap$  symbolizes for the Boolean AND operation. The letters ' $r$ ', ' $g$ ' and ' $b$ ' are used to identify the red, green and blue values respectively. The letters in the subscripts ( $g$ ,  $b$  and  $y$ ) denote the respective intensity values of the RGB for green, blue and yellow pixels. Their values range between 0 (unmixed solution) to 1 (fully mixed solution).

### 3.4 Experimental Setup and Micro-PIV Processing for Droplet Generation

The droplet generation experimentation schematic diagram was shown in Figure 3.5, including microfluidic channel and the associated optical imaging measurement system along with fluid driving mechanism. The droplet behaviours focused at the junction of microfluidic channel were captured using similar model and magnification of microscope used in micromixing having resolution of  $800 \times 600$  pixels. The fluid driving mechanism consisting syringe pump, microcontroller and electronic hardware have already been described in above Section 3.3. The input parameter setting maintained for all the experiments including setting of microscope and initial flow rate was summarized in Table 3.2.

The experiment originally used the Magnaglo<sup>®</sup> 14A fluorescent magnetic powder (mean particle size of 6  $\mu\text{m}$ , manufactured by Magnaflux) suspended in Carrier II (density of 802.837  $\text{kg/m}^3$ , dynamic viscosity of 0.0026  $\text{Pa}\cdot\text{s}$  at 38°C, manufactured by Magnaflux) as dispersed phase, however due to its fast settling in the oil, the preliminary experiments were unsuccessful.

Hence, food grade palm olein having a density of 917  $\text{kg/m}^3$  and viscosity of  $7.97 \times 10^{-2}$   $\text{Pa}\cdot\text{s}$  (Siddique et al., 2010) and distilled water (density of 997  $\text{kg/m}^3$ , viscosity of  $8.90 \times 10^{-4}$   $\text{Pa}\cdot\text{s}$ ) seeded with polystyrene microspheres particles (manufactured by Thermo Scientific<sup>™</sup> 4210A) were respectively injected into inlet A and inlet B for different diameters of offset T-junction microchannels. Food grade palm olein was used as the oil phase due to its high stability index (Idris et al., 2018). The suspension containing seeding particles (Table 3.3) and distilled water with ratio of 1:4 for each experiment. The food grade palm olein and the seeding particles were assumed to have the same density and dynamic viscosity as distilled water.

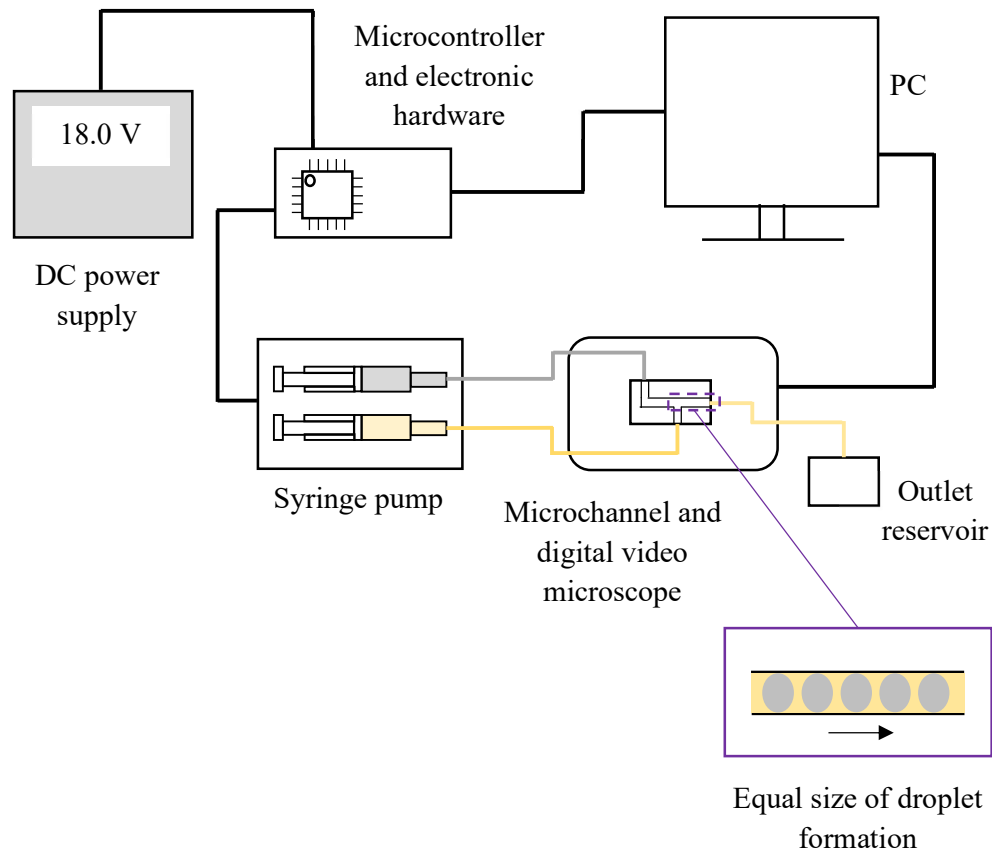


Figure 3.5: Schematic diagram of the experimental setup for droplet generation

Table 3.2: Controlled parameters

Parameter	Value
Exposure time	3.906 ms
Colour temperature	5547
Frame rate	21.8 fps
Resolution	800 × 600 pixels
Motor step	5
Flow rate of liquid at the inlets	0.16 mm <sup>3</sup> /s

Table 3.3: Specification of seeding particle (Turner et al., 2018)

Composition/ Material	Polystyrene
Diameter	10 $\mu\text{m} \pm 0.08 \mu\text{m}$
Concentration	0.2% solids
Density	1.05 $\text{g}/\text{cm}^3$
Refractive index	1.59 at 589 nm (25°C)

By adopting time-resolved as the image sequencing style in micro-PIV for MATLAB software (Thielicke, 2014; Thielicke & Stamhuis, 2014), the flow patterns of the fluids were obtained. The region of interest was set to the whole area of the  $800 \times 600$  pixels frame. For image pre-processing, contrast limited adaptive histogram equalization (CLAHE) was applied to the images for visibility enhancement. Then, the images were processed by cross-correlation function in order to obtain the raw velocity vectors of the liquids. The calibration was performed using the image of 10  $\mu\text{m}$  polystyrene microsphere having resolution of  $6 \times 6$  pixels. The vector validation was done to eliminate some incorrect vectors remaining from noise peaks in the correlation function. The vector and velocity magnitude for each experiment were presented and discussed.

## CHAPTER 4

### RESULTS AND DISCUSSION

#### 4.1 Overview

The first part of Chapter 4 discusses experimental result pertaining to micromixing experiment, while the latter elucidates experimental result of droplet generation experiment.

#### 4.2 Micromixing

##### 4.2.1 Effect of Channel's Design on The Mixing Index of Two Dissimilar Miscible Liquids (Propan-2-ol and Water)

For propan-2-ol and water mixing in T-junction microchannel, the graph (Figure 4.1(a)) indicates that as mixing time increases, mixing index for each Reynolds number also increases until maximum index of 1 is reached. At the early stage of mixing, Reynolds number of 10 shows a steep rising index than the others. This is because higher molecular diffusion takes place while the flow rate is low due to its higher residence time (Mondal et al., 2020). Figure 4.2(a) shows that propan-2-ol and water do not flow side by side in the low Reynolds number regime as there is a large amount of mass transfer perpendicular to the main flow (Wang et al., 2012). At  $Re = 5$ , it can be seen that the mixing process is slower to take effect at the early stage but as the diffusion time increases, the mixing quality of propan-2-ol and water also increases. However, at  $Re = 30$ , the less residence time for diffusion transport results in poor mixing performance at a fixed position (Wang et al., 2012), which can be observed from 0 to 0.375 s. Meanwhile, at high Reynolds number of 40 and 50, maximum index of 1 is reached in the shortest time at 0.25 s. The process is dominated by massive convection process which is occurred when stratified flow changed to vortex flow (Wang et al., 2012). With the increase of Reynolds number, the momentum also

increases resulting in circulation in wider regions of flow and produced a local maximum velocity (Chung & Shih, 2008) from 0.0030 m/s ( $Re = 5$ ) to 0.0298 m/s ( $Re = 50$ ). The effect of induced circulation results in efficient mixing of propan-2-ol with water as the circulation provides further increased interfacial area as well as better advection (Chung & Shih, 2008). The efficiency of mixing then remains at 100%. The experimental results of propan-2-ol and water mixing in the T-junction microchannel are much similar to the reported experimental result of Wang et al. (2012), where ethanol and water are being experimented in the T-junction microchannel.

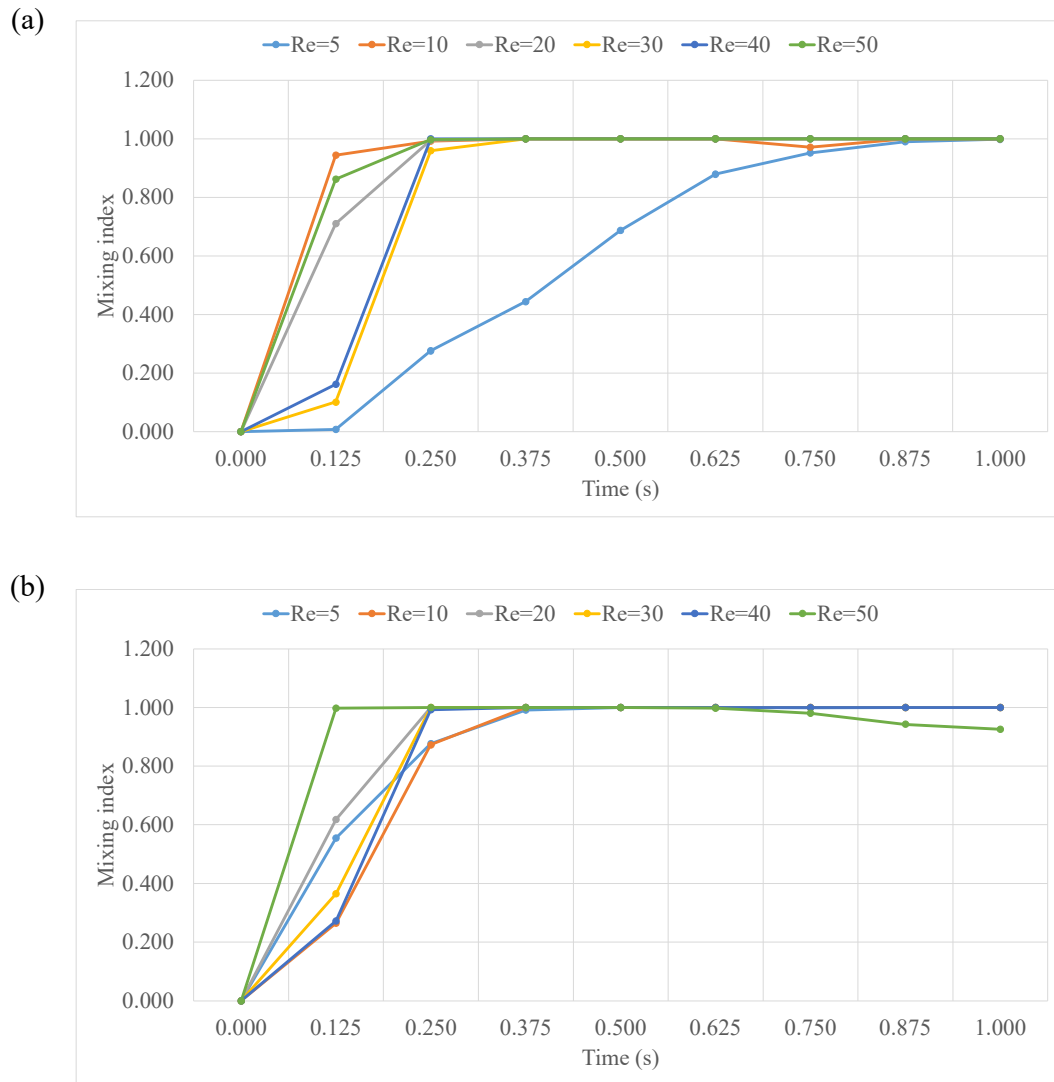


Figure 4.1: Mixing index of propan-2-ol and water at (a) T-junction, and (b) offset T-junction

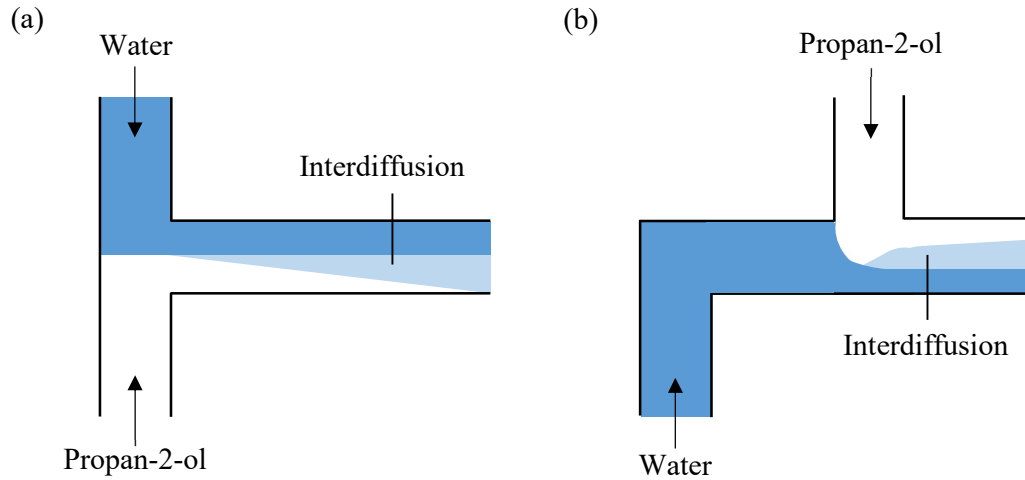


Figure 4.2: Top view indicating schematically the interdiffusion layer of miscible propan-2-ol-water micromixing in (a) T-junction and (b) offset T-junction microchannels

Based on Figure 4.1(b), the graph of mixing in offset T-junction microchannel has the same pattern with the ones in the T-junction microchannel, where mixing index increases with the mixing time. At low Reynolds number of 5 and 20, propan-2-ol diffuses into water quickly due to the concentration difference for liquid-liquid mass transfer (Wang et al., 2012). For medium Reynolds number of 30, the mixing performance at the early stage of mixing is found similar to the previous propan-2-ol and water experiment in T-junction microchannel. At high Reynolds number, the experimental results of propan-2-ol and water mixing within offset T-junction microchannel is fitted the explanation of reported experimental result of Wang et al. (2012), where ethanol and water are being experimented in the offset T-junction microchannel. The propan-2-ol stream is pushed to the center of the channel owing to its inertia while the water stream is moved towards the walls of the channel in the premises of the convergent junction of the two flow inlets (Wang et al., 2012) as illustrated in Figure 4.2(b). At  $Re = 50$ , mixing index increases and after half second, it starts

to decline. Nevertheless, the highest mixing index of 1 is fastly achieved at this Reynolds number around 0.25 s. This is because at high Reynolds number, the interfacial area between propan-2-ol and water increases due to high liquids velocity. As a result, the convective diffusion compared to molecular diffusion, owing to the liquid lamellae stretching and subsequent thinning (Wang et al., 2012), dominates the mixing process.

#### **4.2.2 Effect of Channel's Design on The Mixing Index of Two Dissimilar Miscible Liquids (Water and Sodium Chloride Solution)**

Figure 4.3(a) illustrates mixing index of water and sodium chloride solution, for each Reynolds number in T-junction microchannel, is directly proportional to the mixing time. At the early stage of mixing around 0.125 s to 0.375 s, the mixing index values increase as Reynolds number increases. The result of rising the Reynolds number at the T-junction of the microchannel is the generation of vortices at junction (Ansari et al., 2018). This vortex generation stretches and increases the interface area of the two streams. At the same time, the factor of viscosity and density difference starts to show its impact. Sodium chloride solution with a higher viscosity and density pushes the less viscous and less dense water from the channel walls and somewhat envelops it (Lobasov et al., 2016) as shown in Figure 4.4(a). This resulted in an increase of the interface area of miscible liquids and consequently enhance the mixing in this regime (Lobasov et al., 2016). Unlike previous experiment of propan-2-ol and water mixing process, especially at low Reynolds number of 5, it can be seen that the liquids are not yet fully mixed at 1 s due to the very slow molecular diffusion. A well-mixed state for this Reynolds number can be achieved after a long enough mixing time (Wang et al., 2012).

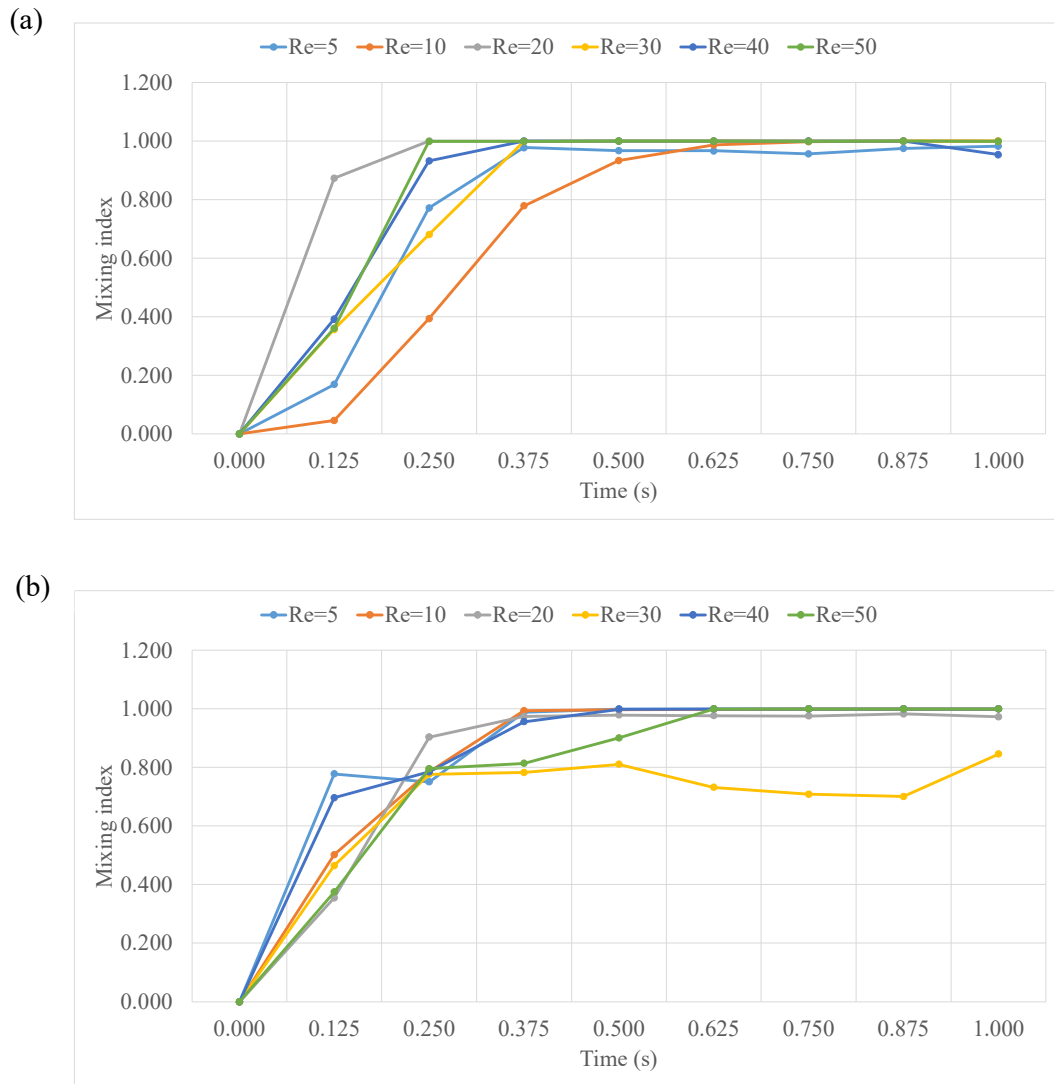


Figure 4.3: Mixing index of water and sodium chloride solution at (a) T-junction, and (b) offset T-junction

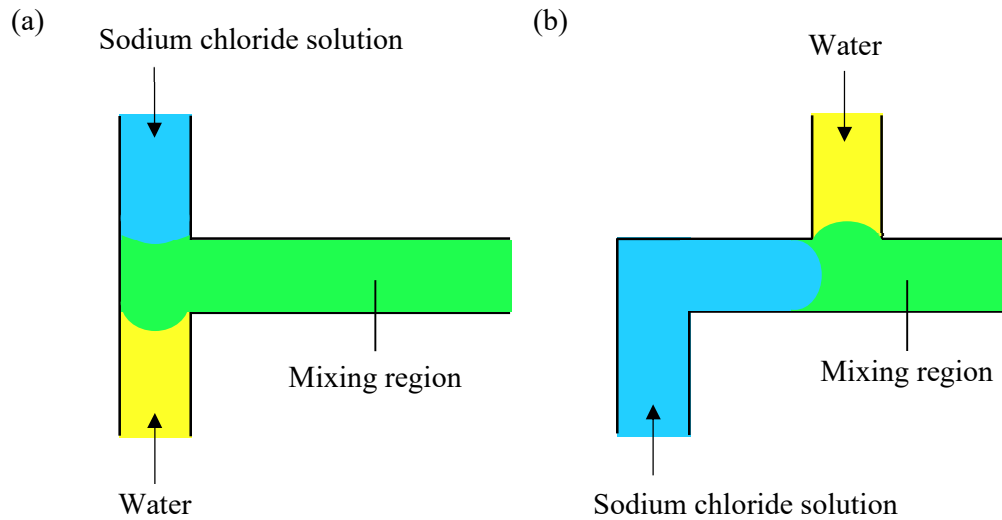


Figure 4.4: The schematic diagram mixing of water and sodium chloride solution in (a) T-junction, and (b) offset T-junction microchannels

Meanwhile, for offset T-junction microchannel, mixing index dropped at 0.5 s then rose again at 1 s at medium Reynolds number of 30 shown in Figure 4.3(b). Compared to previous mixing experiment of same liquids in T-junction microchannel, very poor mixing between water and sodium chloride solution can be observed at this medium range of Reynolds number. With the increasing values of Reynolds numbers, the residence mixing time is lowered and enhanced inertial effects lead to decrease in mixing performance of water and sodium chloride solution (Wang et al., 2012) from  $Re = 5$  to  $Re = 30$ . On the other hand, at high Reynolds number of 40 and 50, the mixing index increases due to the transition of the flow pattern, which is from stratified to vortex flow (Wang et al., 2012). At low as well as high values of Reynolds numbers, the mixing performances are better in comparison to medium Reynolds number. At high Reynolds number, the mixing performance is good due to the massive convection caused by the effect of stretching and thinning of liquid

lamellae and wrapping of two liquid lamellae yield and enlarged the interfacial surface area (Wang et al., 2012) as shown in Figure 4.4(b).

#### **4.2.3 Effect of Channel's Design on The Mixing Index of Two Dissimilar Immiscible Liquids (Propan-2-ol and Sodium Chloride Solution)**

Based on Figure 4.5(a), in T-junction microchannel, at low Reynolds number of 5, 10 and 20, as time increases, mixing index also increases but after 0.25 s, the values for  $Re = 10$  and  $Re = 20$  drop and then rise again. Meanwhile, at medium and high Reynolds number of 30, 40 and 50, the mixing index keeps fluctuating as it drops and rise repetitively. In fact, the molecular diffusion process between immiscible propan-2-ol and sodium chloride solution is difficult compared to the previous two miscible mixing experiments. Because of the fact that the salt ions are smaller in size, water molecules displace the alcohol molecules in solvating these ions (Fang et al., 2018). The molecular attraction between salt ions and water molecules is much stronger compared to alcohol owing to the fact that alcohol is less polar than its counterpart. This results in formation of bonds between all of the water molecules and salt ions, resultantly providing no opportunity to form hydrogen bonds with the alcohol (Fang et al., 2018). As a result, the water-salt solution becomes immiscible with propan-2-ol and thus forms a separate layer.

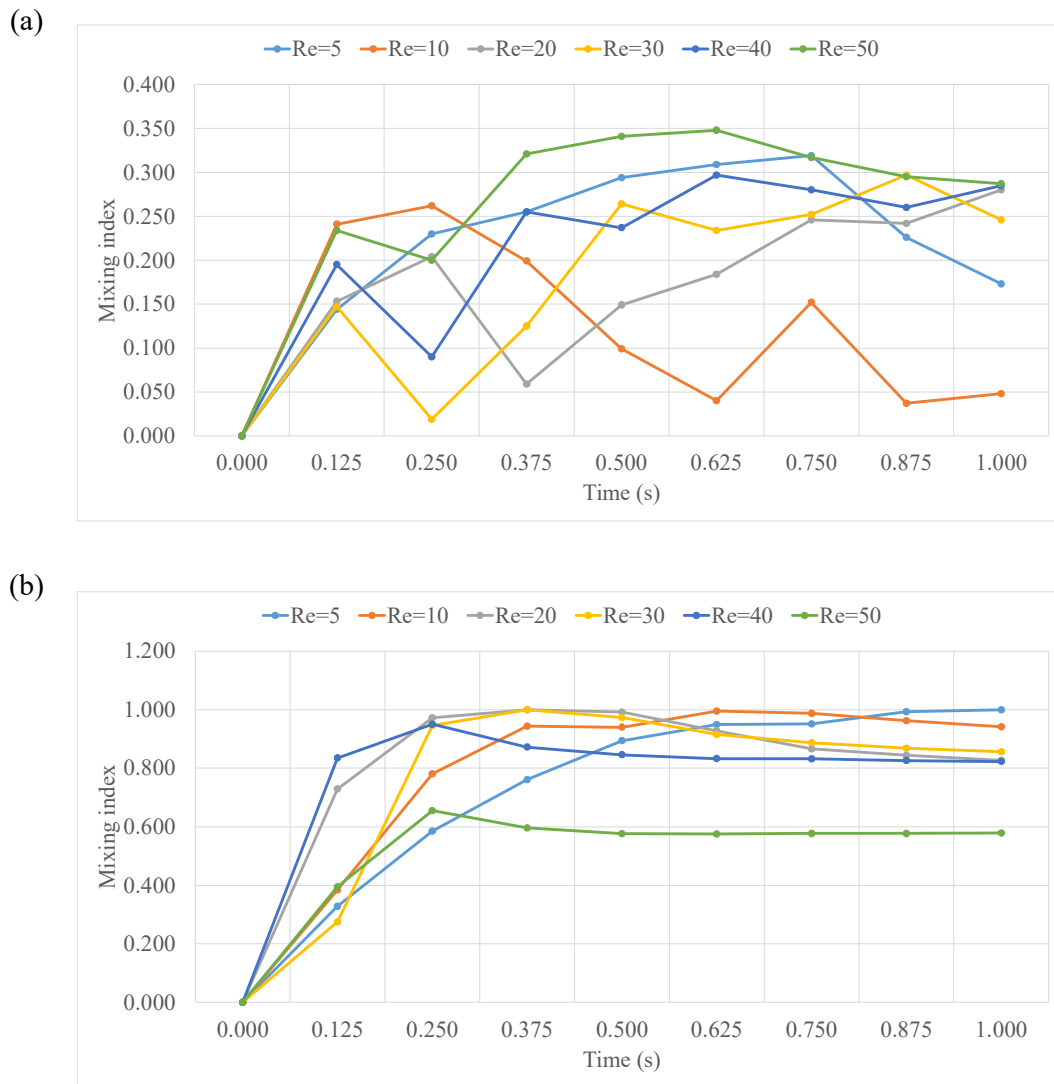


Figure 4.5: Mixing index of propan-2-ol and sodium chloride solution at (a) T-junction, and (b) offset T-junction

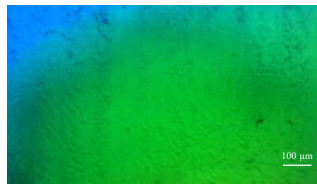
Figure 4.5(b) illustrates mixing index of propan-2-ol and sodium chloride solution for each Reynolds number in offset T-junction microchannel increases as time increases, but after half second, most of the value declines. This is owing to the competition between the salt ion and alcohol molecules for the water molecules (Fang et al., 2018). Since, for alcohol

molecules, fewer water molecules are available to form the hydrogen bonds; propan-2-ol remains lesser soluble in the mixture. At the end, the propan-2-ol forms a separate layer on top of the mixture (Fang et al., 2018). The two layers are easily recognizable since both have different colors as the water layer remains clearer while ‘greenish-blue’ alcohol layer is seen in this experiment as seen in Figure 4.6. It concludes that the dye inks are more soluble in the propan-2-ol. Compared to the immiscible mixing experiment performed in the T-junction microchannel earlier, this graph shows better pattern of mixing within offset T-junction microchannel.



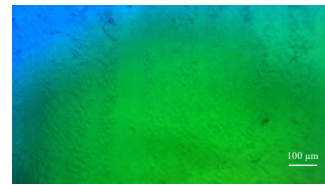
$t = 0.375 \text{ s}$

$MI = 0.872$



$t = 0.500 \text{ s}$

$MI = 0.846$



$t = 0.625 \text{ s}$

$MI = 0.833$



$t = 0.750 \text{ s}$

$MI = 0.832$



$t = 0.875 \text{ s}$

$MI = 0.826$



$t = 1.000 \text{ s}$

$MI = 0.823$

Figure 4.6: Actual mixing images (1400  $\mu\text{m}$  length and 790  $\mu\text{m}$  width) of blue dye in propan-2-ol and yellow dye in sodium chloride solution within offset T-junction microchannel at Reynolds number of 40. MI stands for mixing index.

The mixing behavior of two different liquids in T-junction and offset T-junction microchannels are compared. Due to dissimilar geometry, the considerable factor that may affect the initial mixing process is momentum difference between liquids at inlets (Wang et al., 2012). Based on Figure 4.7, offset T-junction microchannel offers better mixing of propan-2-ol and sodium chloride solution compared to T-junction microchannel at both low and high Reynolds number. The chaotic mixing happened within the T-junction microchannel due to the direct interaction of two liquids entering the junction at high momentum. When the inlets of T-junction having an offset of 7.5 mm, the mixing quality increases by twice or more. The inlet stream has, to some extent, the synergetic effect with molecular diffusion (Wang et al., 2012). At Reynolds number of 5, the highest mixing index at T-junction microchannel is 0.3 meanwhile offset T-junction microchannel is 1. Besides that, at high Reynolds number, the index reading at offset T-junction microchannel is twice the value of index at T-junction microchannel. However, the synergetic effect along with residence time is reduced with the increased flow rates (Wang et al., 2012). Therefore, the diffusion between two streams decreases. From the graph, mixing quality of propan-2-ol and sodium chloride solution at low Reynolds number is much better than at the Reynolds number of 50. At both high and low Reynolds numbers, the well-mixing behavior between propan-2-ol and sodium chloride solution is highly achieved using offset T-junction microfluidic channel.

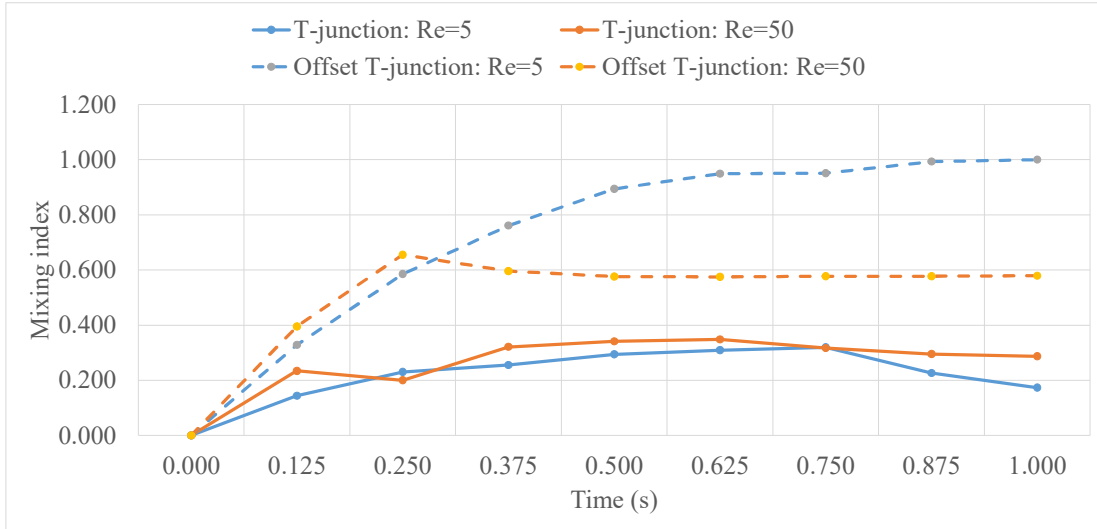


Figure 4.7: Comparison of mixing index between propan-2-ol and sodium chloride solution at different Reynolds number in T-junction and offset T-junction microchannels

### 4.3 Droplet Generation

Based on the earlier experimental results, microfluidic offset T-junction offers better performance than the T-junction channels. For this reason, the behaviours of distilled water droplet formation suspended in food grade palm olein at interfacial surface was investigated using offset T-junction microchannels having radius of 400  $\mu\text{m}$ , 500  $\mu\text{m}$ , 750  $\mu\text{m}$  and 1000  $\mu\text{m}$  via micro-PIV software.

#### 4.3.1 Evolution of Water Droplets at The Junction of Offset T-microchannel

In general, less viscous water flows faster than more viscous oil. However, when both solutions experimented in a microchannel, the superhydrophobic coating on the walls of the channel creates a small air gap between the inside wall of the channel and the outer surface of the liquids (Vuckovac et al., 2020). The air gap around more viscous liquid is larger, which allowed food grade palm olein to move through the channel faster than the less viscous distilled water.

Figure 4.8 shows the growth of water droplets at the junction in an offset T-microchannel at time =  $t$ . From the figure, the size of the droplets is increasing as the diameter of microchannel increases. The water droplet is rounder and more solid-shaped within microchannel's radius of  $750\ \mu\text{m}$ . Its size is less than or nearly equal to the microchannel's width. When the droplet reached the junction, the oil pushed the water droplet upwards and cause an irregular shape at the bottom of the droplet as can be seen at  $t = t_3$ . At this point, the droplet is likely starting to be in the break-up process. The droplet expanded mainly in radial direction and slightly in axial direction (Fu et al., 2009). Hence, the length increases gradually while the width increases moderately. This point is named as thread expansion stage and the period is called expansion time (Fu et al., 2009). As it reached  $t = t_4$ , the cross-flowing liquids drove the thread in its axial direction and a visible neck formed.

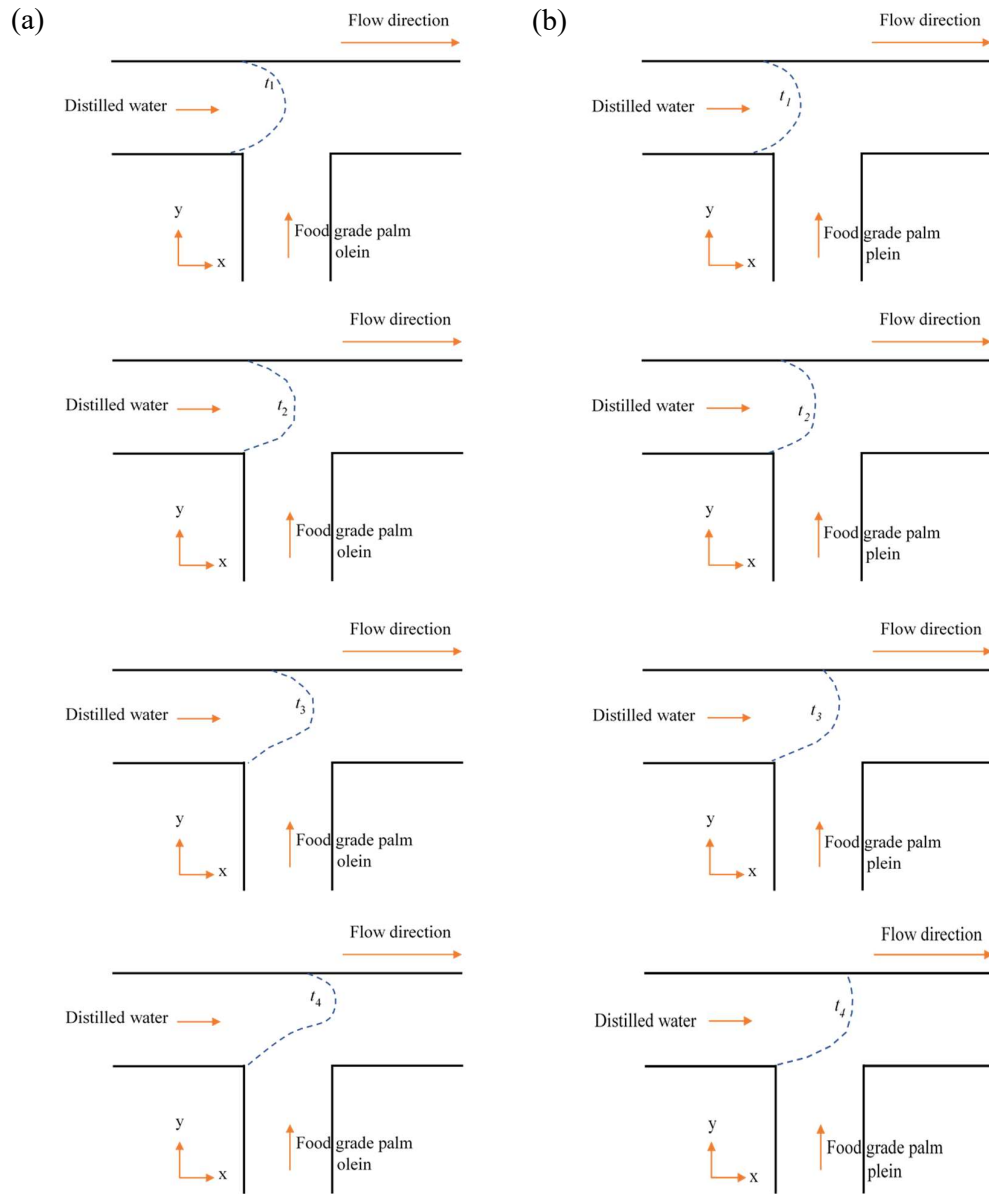


Figure 4.8: The evolution of water droplets for offset T-microchannels with radius of (a) 400  $\mu\text{m}$ , and (b) 750  $\mu\text{m}$

### 4.3.2 Experimental Velocity of Water Droplets at The Junction of Offset T-channel

Figure 4.9 shows the motion of droplets in the offset T-junction microchannels from  $t = 91 \text{ ms}$  to  $t = 455 \text{ ms}$ , while Table 3 summarizes the minimal difference in theoretical and

experimental velocity of the water droplets. Increasing in the radius of offset T-junction microchannel leads to the decrease of droplet's velocity. Velocity decreases when the cross-sectional area increases (Pang et al., 2014). This is a consequence of the continuity equation. If the flow rate is held constant, when the area decreases, the velocity must increase proportionally. Based on Table 4.1, the experimental data have proved this theory, where microchannel with radius 400  $\mu\text{m}$  has higher water droplet's velocity than the channel with radius 750  $\mu\text{m}$ .

The experimental velocity of the distilled water phase's also holds a good agreement with the ones that theoretical have. The surface roughness of the channel walls might affect the liquids' flows, which cause 0.06 mm/s difference in theoretical and experimental velocity of the distilled water phase within microchannel radius of 500  $\mu\text{m}$ . However, the actual roughness of the walls could not be quantified. For the inlet and outlet radius of offset T-junction microchannel = 1000  $\mu\text{m}$ , the experimental velocity could not be determined due to the droplet was forming outside the field of view as the image was maintain captured at the junction.

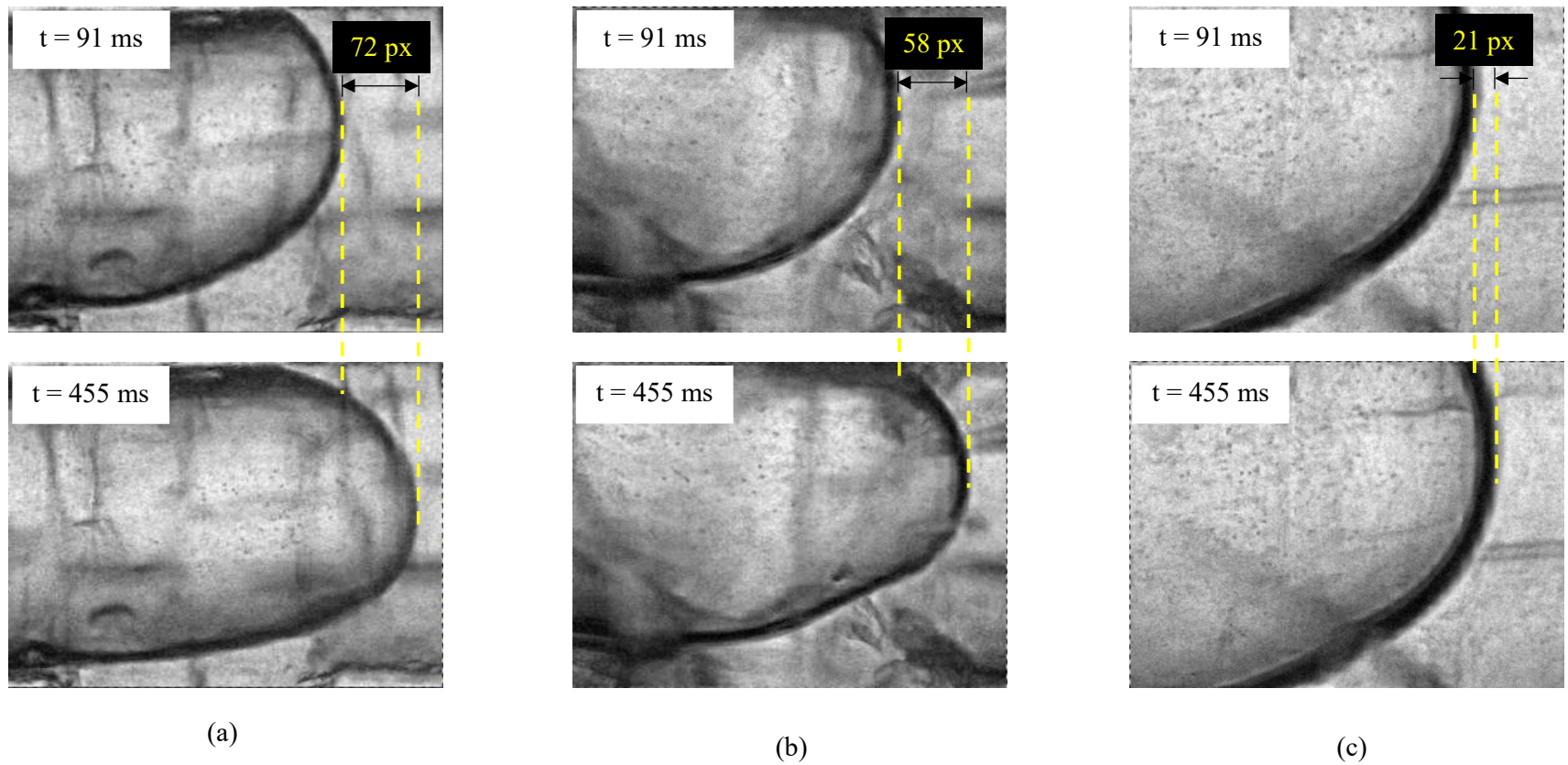


Figure 4.9: The motion of water droplets after 364 ms within radius of (a) 400  $\mu\text{m}$ , (b) 500  $\mu\text{m}$ , and (c) 750  $\mu\text{m}$  offset T-microchannels

Table 4.1: Theoretical and experimental velocity of water droplets

Inlet and outlet radius of offset T-junction microchannel ( $\mu\text{m}$ )	Theoretical velocity based on Reynolds number (mm/s)	Experimental velocity (mm/s)
400	0.322	0.330
500	0.206	0.266
750	0.092	0.096
1000	0.051	

### 4.3.3 Internal Velocity Profile of Generated Water Droplets

Figure 4.10 to Figure 4.13 show pre-processing images, vector analysis and also velocity magnitude analysis performed by micro-PIV technique via MATLAB software for the droplet flow and slug flow pattern. As the water is dispersed phase, the superhydrophobic coating promotes these dispersed flows in which the water phase must wet the wall of the microchannel (Vuckovac et al., 2020).

The pattern of the flow involving droplets as shown in Figure 4.10 to Figure 4.12 can be characterized by the sub-channel sized droplets (Darekar et al., 2017). The formation of such droplets, having diameter less than channel diameter, are generated at low dispersed and high continuous phase flow rates. In such conditions, the inertial force input at the higher flow rate of the continuous phase is high enough to break down the dispersed phase into smaller droplets with lesser resistance posed by the dispersed phase at lower flow rate. Meanwhile, for the slug flow pattern which is likely to be the flow behaviour for microchannel with radius 1000  $\mu\text{m}$  (Figure 4.13), the slug occupied almost the whole cross-section of the microchannel with a very thin layer of the oil phase between the slug and the

wall of the offset T-junction microchannel. However, the shear stress is not significant in this regime and the interfacial tension along with the pressure gradient results in the breakup of dispersed phase into slug. Resultantly, the slug growth leads to the obstruction to the continuous phase flow (Darekar et al., 2017).

In terms of the microchannel's size affecting the size of droplet, based on Figure 4.10 to Figure 4.12, the droplets' size increases with an increase in the radius of the microchannels (Kashid & Agar, 2007). In the case of small differences between the offset T-junction microchannels i.e., radius of 400  $\mu\text{m}$  and 500  $\mu\text{m}$ , there is no major difference in droplets' sizes can be spotted from Figure 4.10 and Figure 4.11. However, with further increase in the microchannel's radius to 750  $\mu\text{m}$  (Figure 4.12), the water droplet's size with respect to flow velocity increases significantly. For the microchannel with radius of 1000  $\mu\text{m}$  (Figure 4.13), the droplet's volume cannot be seen due to the limit of field of view and the exceedance of the observation area. From this discussion, it is clear that the change in the offset T-junction microchannel's radius exerts a major influence on the water droplet's size.

On the other hand, in the aspect of flow velocity, at  $t = 91 \text{ ms}$  and  $t = 1000 \text{ ms}$ , microchannel with radius of 750  $\mu\text{m}$  (Figure 4.12) has average velocity of 0.055 mm/s and 0.15 mm/s which is 2.7 and 1.3 times smaller than the average velocity of microchannel with radius of 500  $\mu\text{m}$  (Figure 4.11), respectively. This is because in a bigger channel, the oil phase is eventually taking longer time to break down the water phase into longer slugs. In contrast to that, for a smaller channel, an increase in the velocity with respect to time increases its inertial force which leads to the enhancement in its tendency to break down the water phase into smaller droplets form. In short, increasing the channel's diameter and cross-sectional area decrease the liquid's velocity compared to the ones in the smaller channel.

This also can be proved by referring to the Hagen-Poiseuille equation (Liu & Pang, 2015) below:

$$Q_{HP} = \frac{\pi R^4 \Delta p}{8 \mu L} \quad \text{Equation 4.1}$$

where  $Q_{HP}$  is flow rate,  $R$  is the channel's radius,  $\Delta p$  is the pressure drop between the inlet and outlet,  $\mu$  is the dynamic viscosity of the fluid, and  $L$  is the channel's length.

The velocity could then be shown as,

$$v_{HP} = \frac{Q_{HP}}{A} = \frac{R^2 \Delta p}{8 \mu L} \quad \text{Equation 4.2}$$

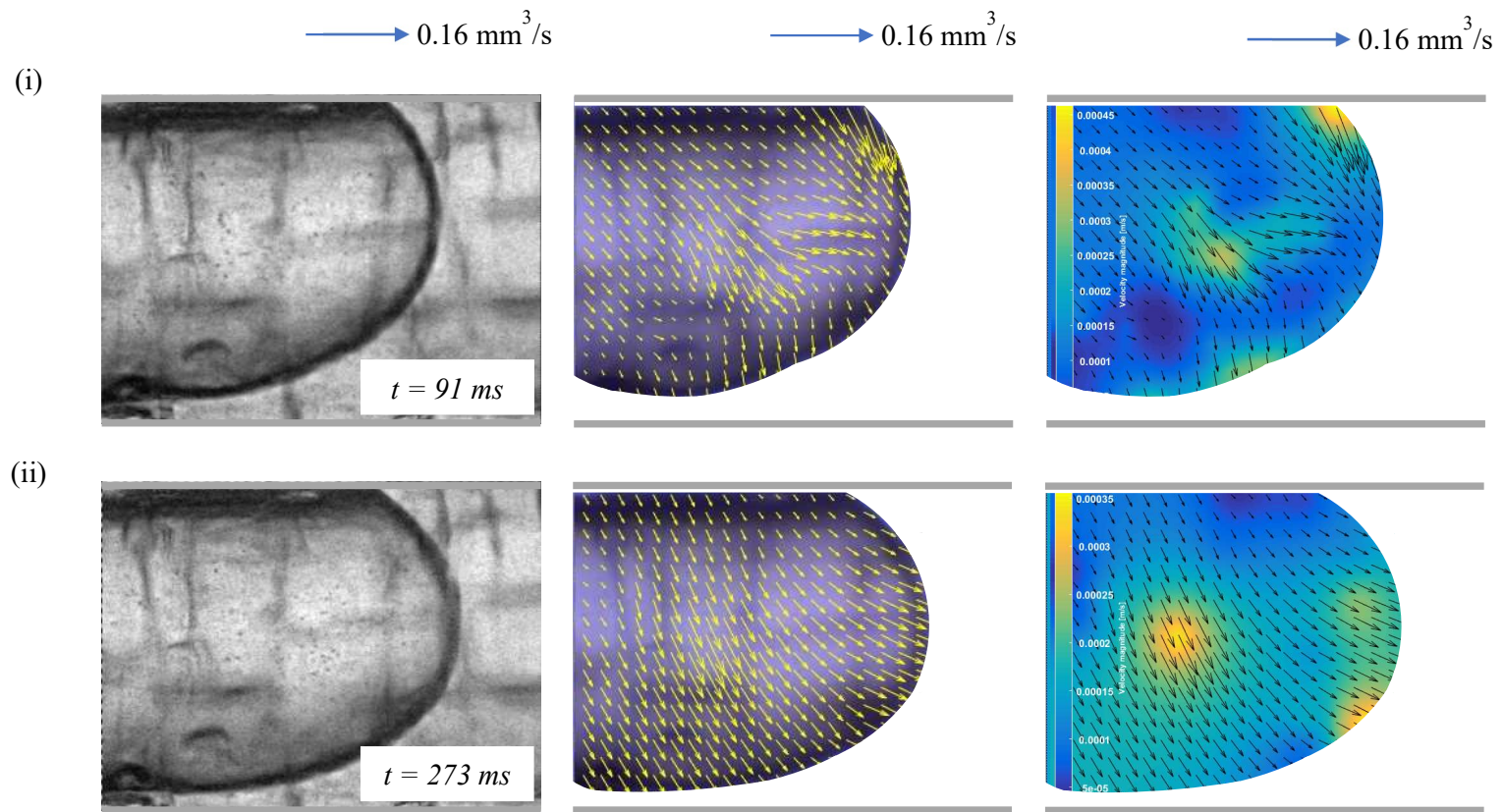
where  $v_{HP}$  is the average velocity,  $A$  is the channel's cross-sectional area.

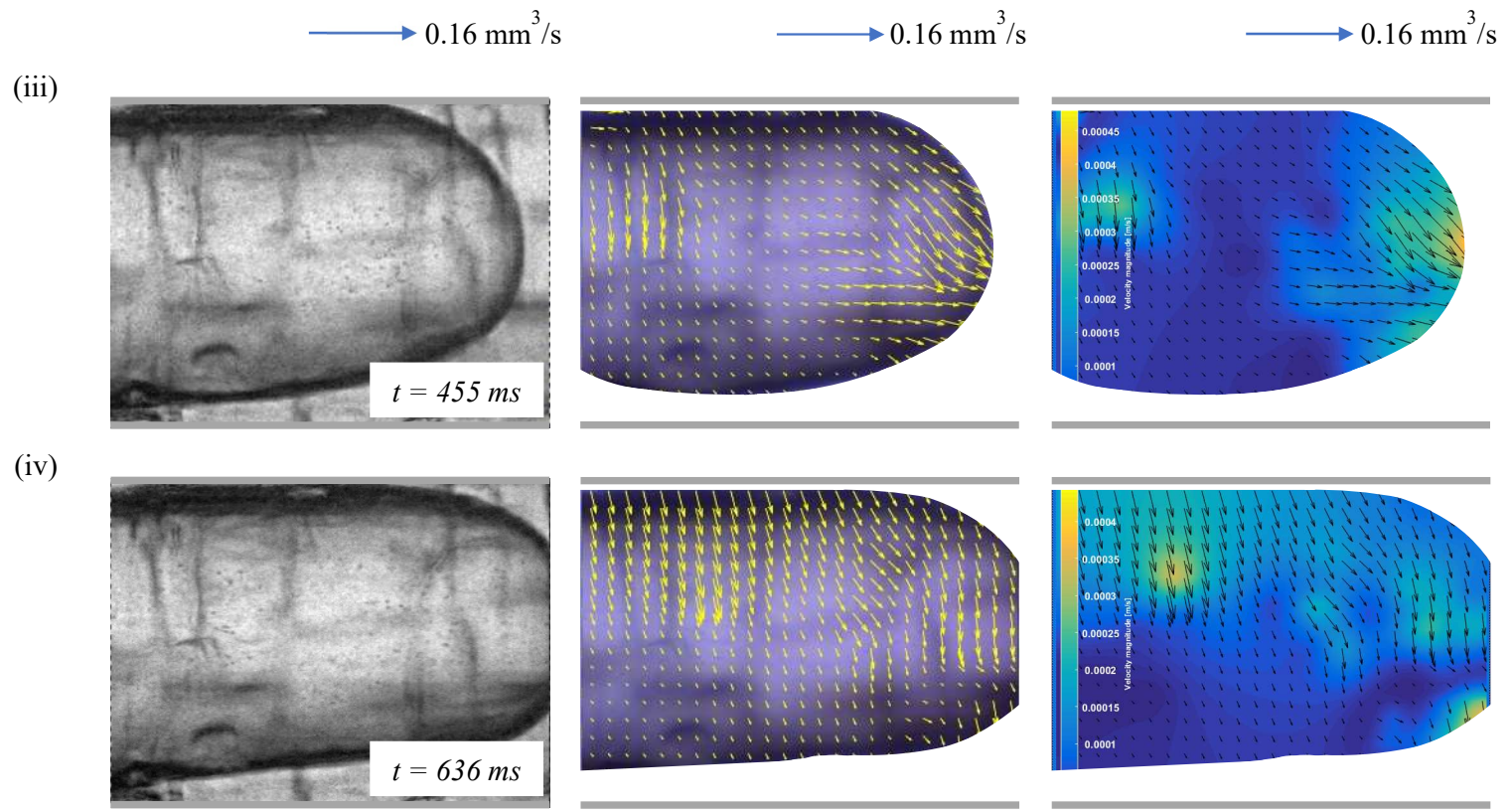
Let  $Q_{exp}$  to be the flow rate measured in the experiment, the velocity can thus be written as,

$$v_{exp} = \frac{Q_{exp}}{A} \quad \text{Equation 4.3}$$

The highest velocity which coloured in yellow region in velocity magnitude analysis is highly due to the vortex which localised near towards the edge of the droplet, as the droplet growing bigger and the particles also moved to the edge. There might be minimal errors in the readings due to the channel's inner geometry and its surface roughness during the fabrication process.

(a) radius of 400  $\mu\text{m}$  offset T-microchannel





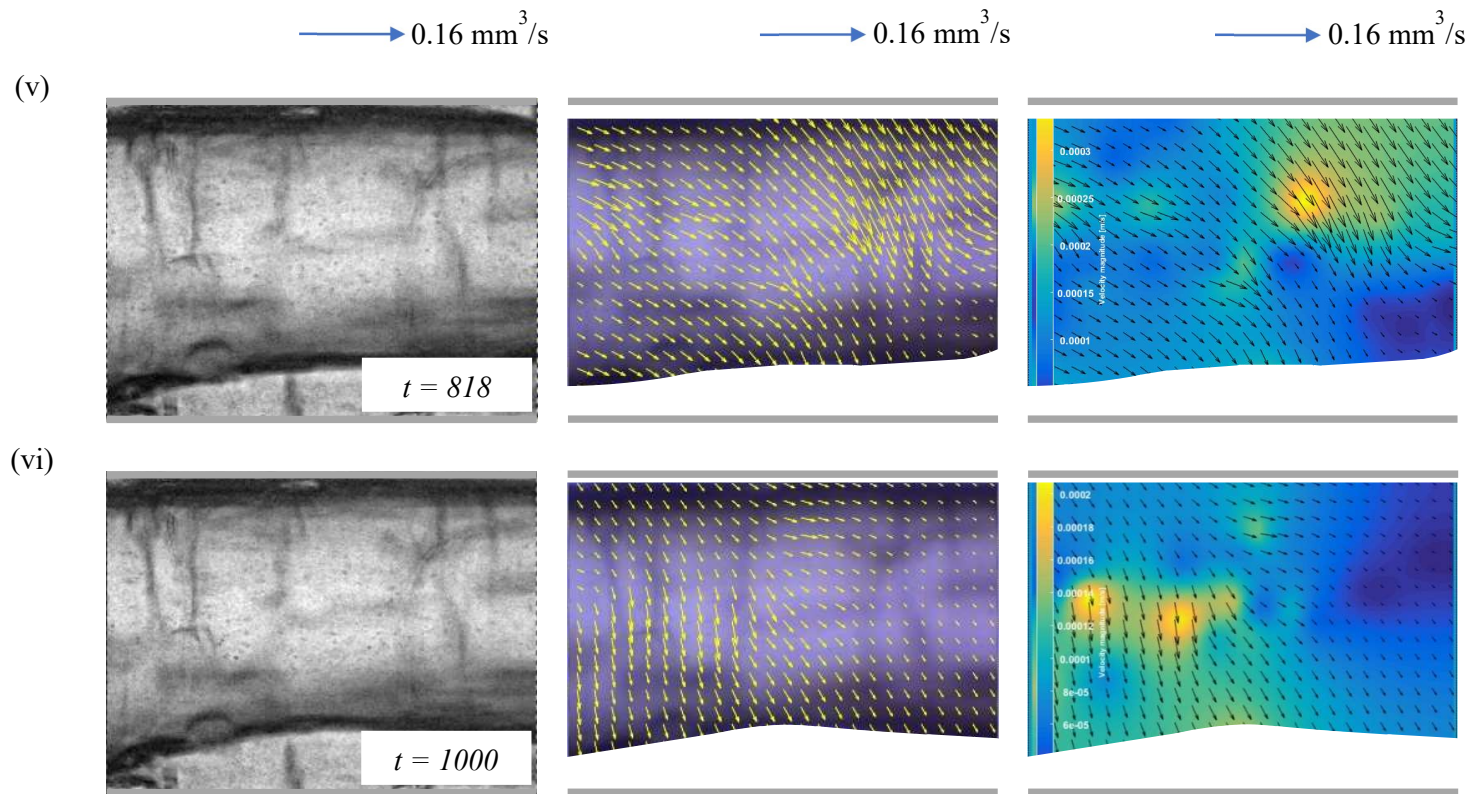
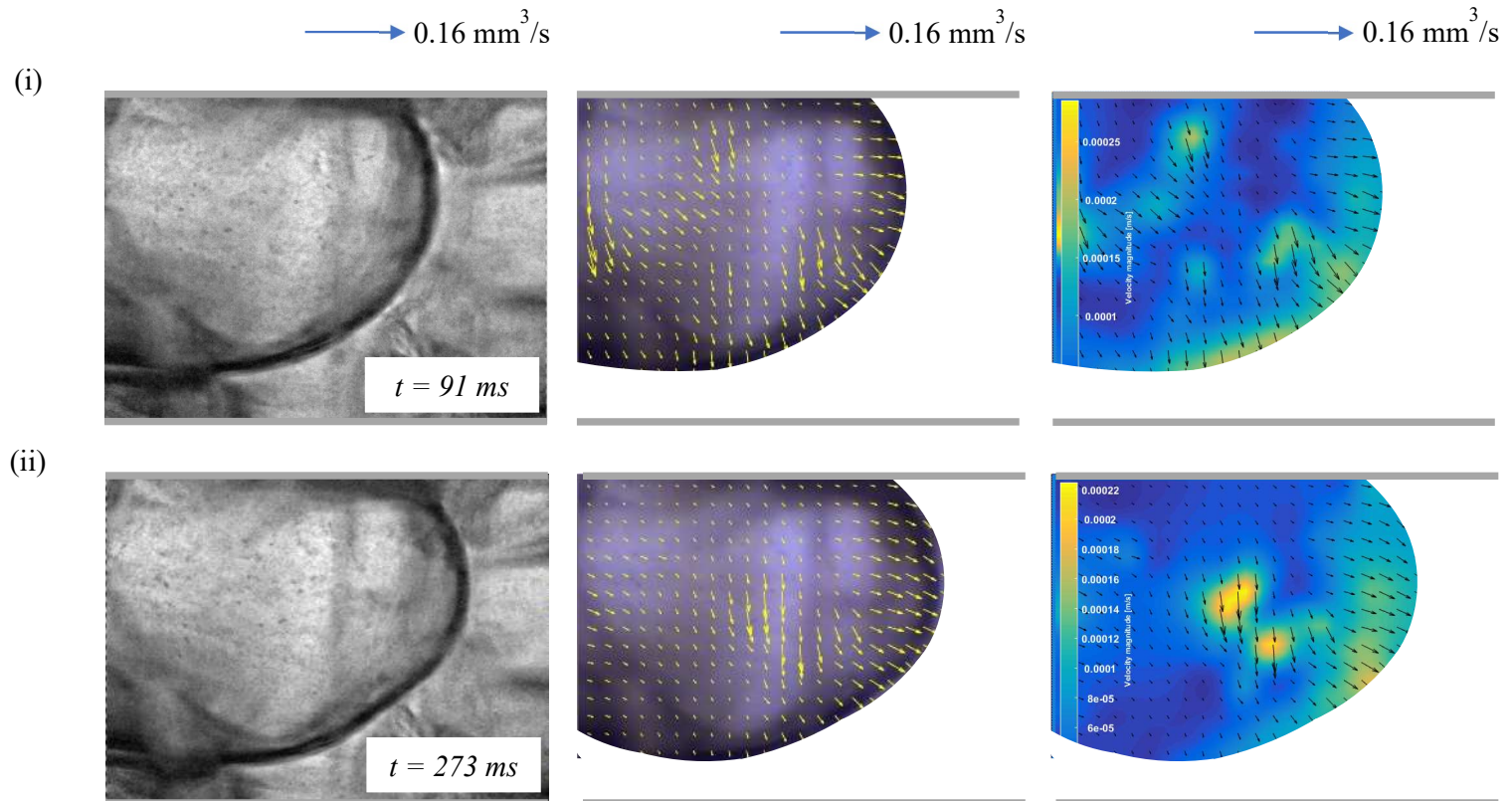
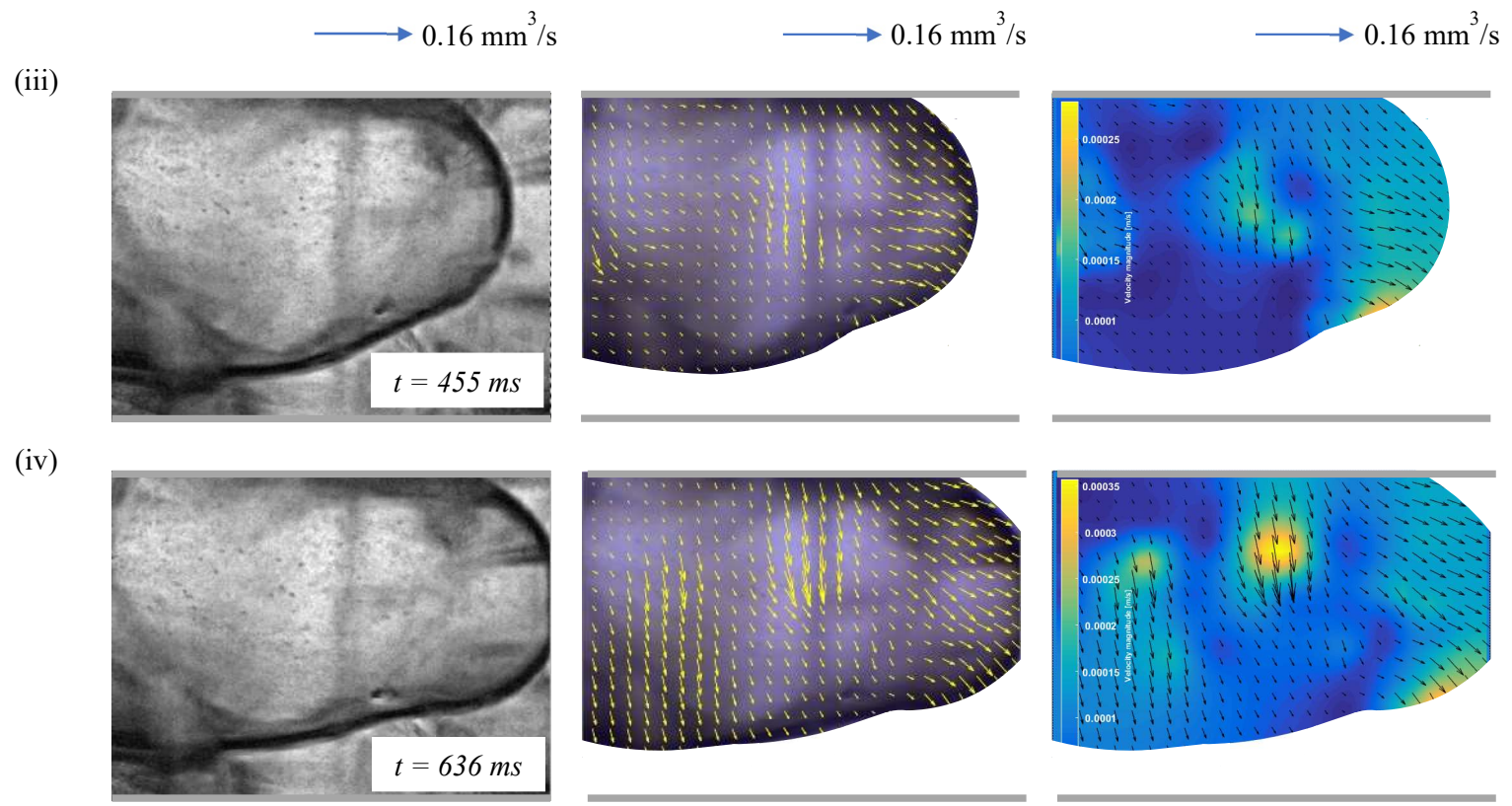


Figure 4.10: Internal velocity profile of generated water droplet for offset T-microchannel with radius of  $400 \mu\text{m}$

(b) radius of 500  $\mu\text{m}$  offset T-microchannel





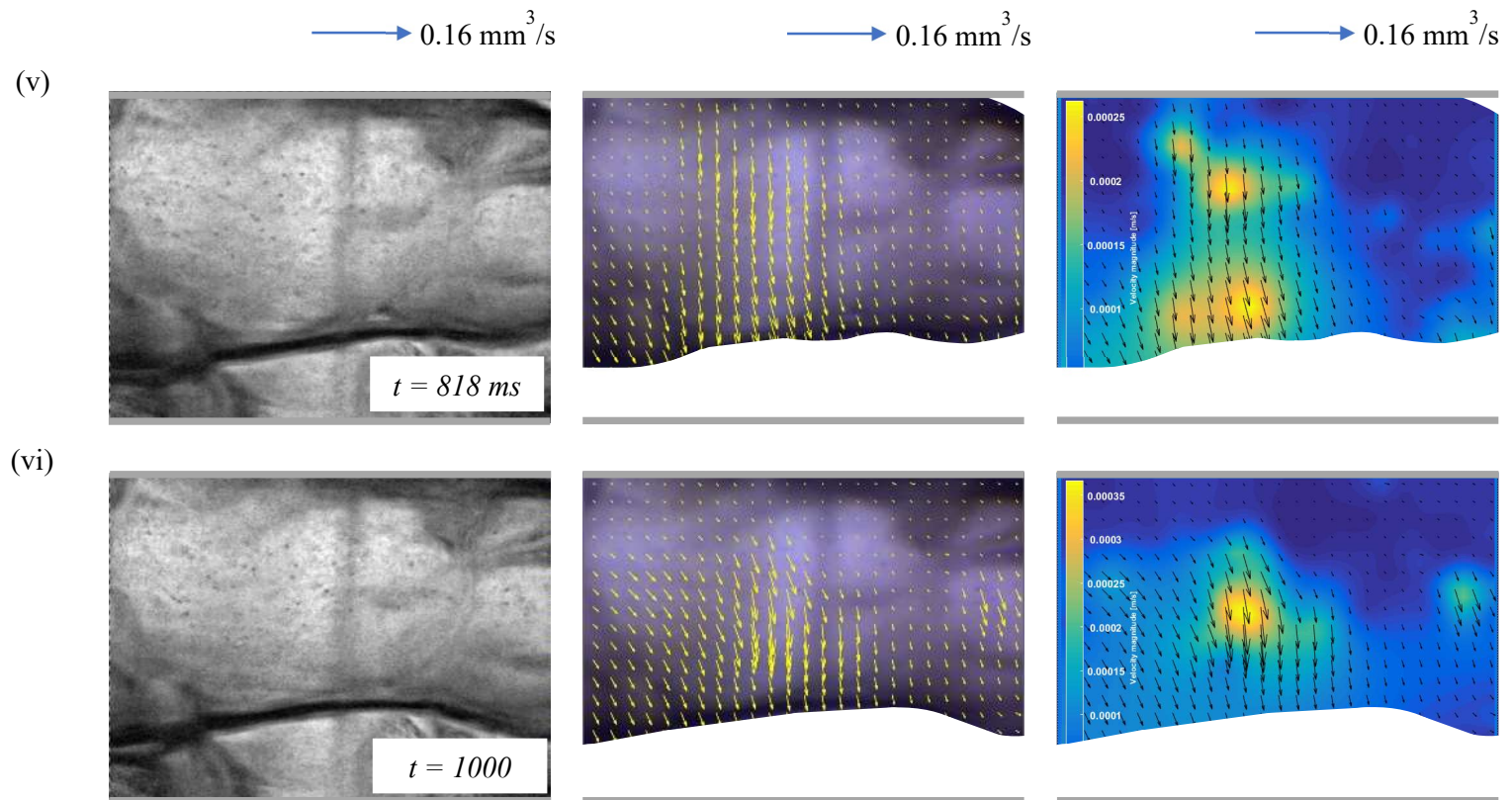
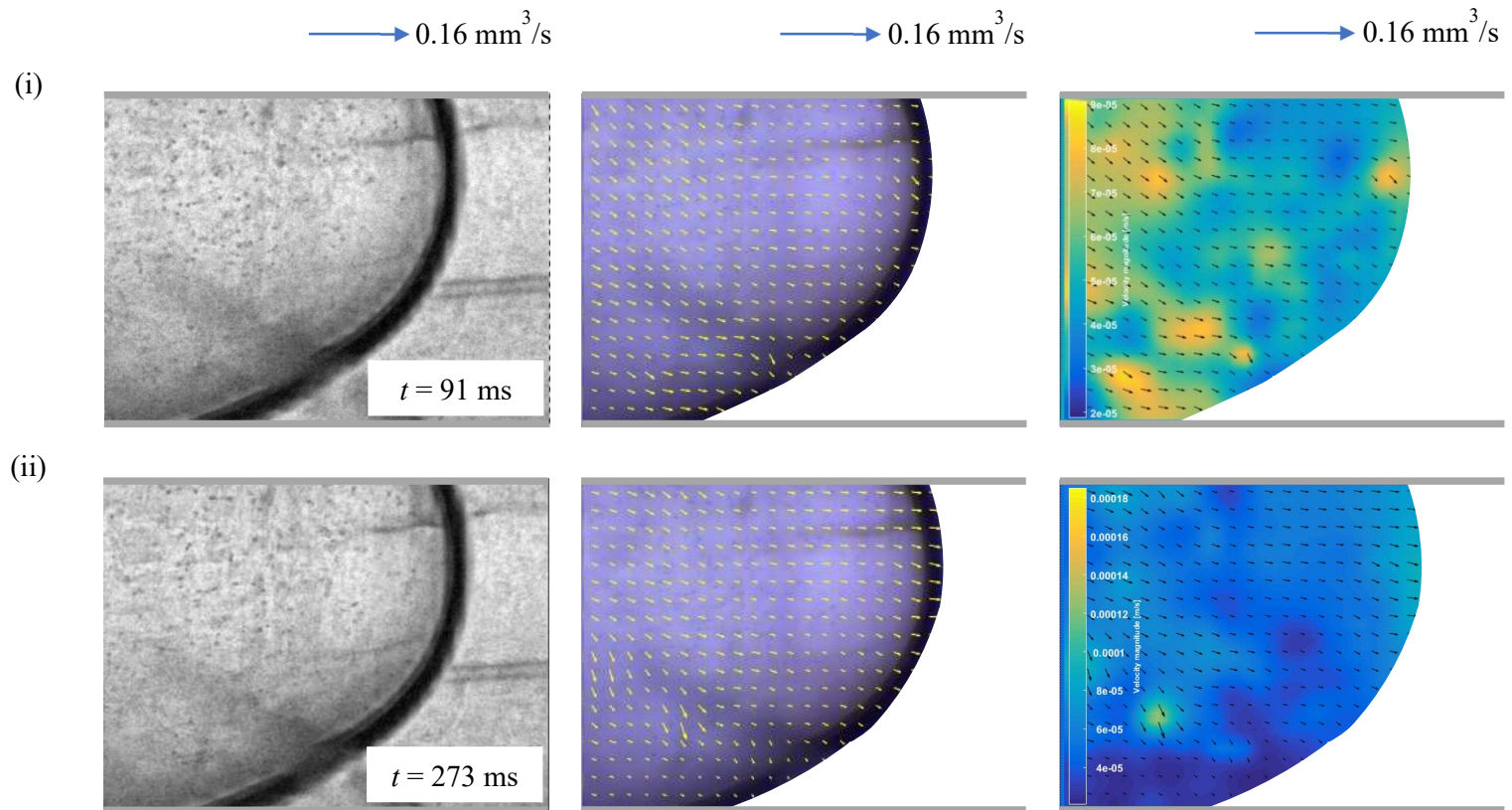
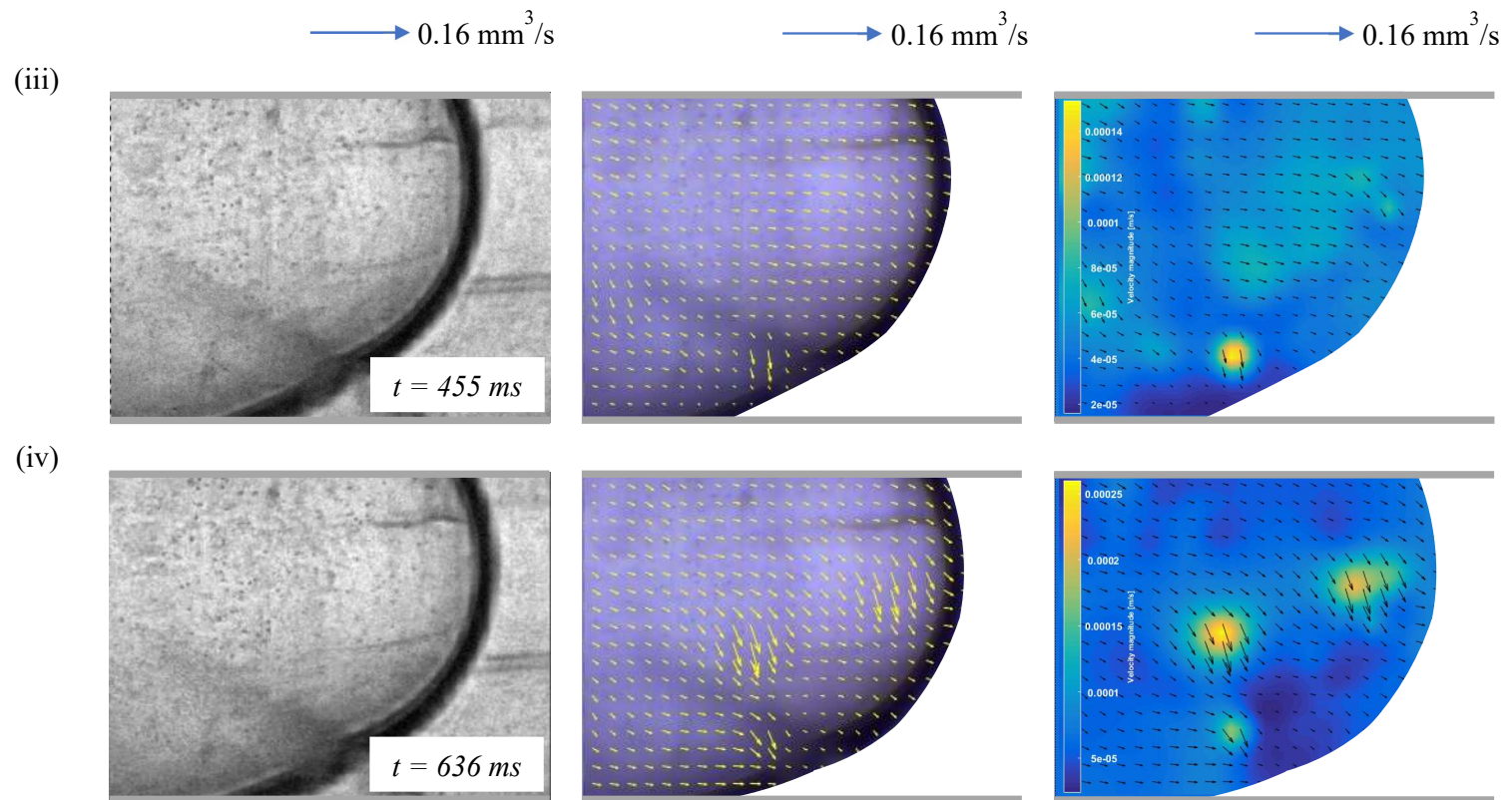


Figure 4.11: Internal velocity profile of generated water droplet for offset T-microchannel with radius of  $500 \mu\text{m}$

(c) radius of 750  $\mu\text{m}$  offset T-microchannel





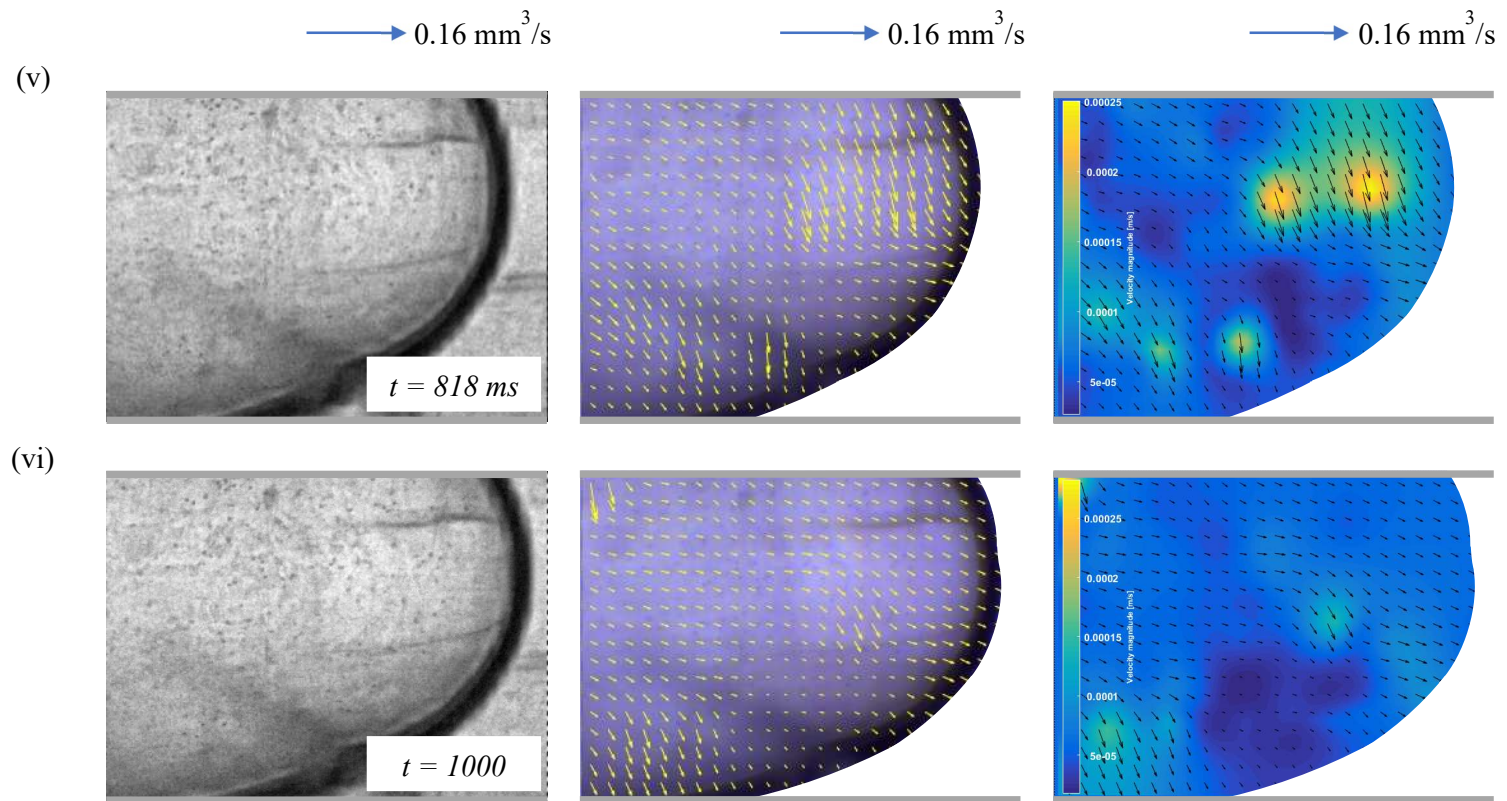
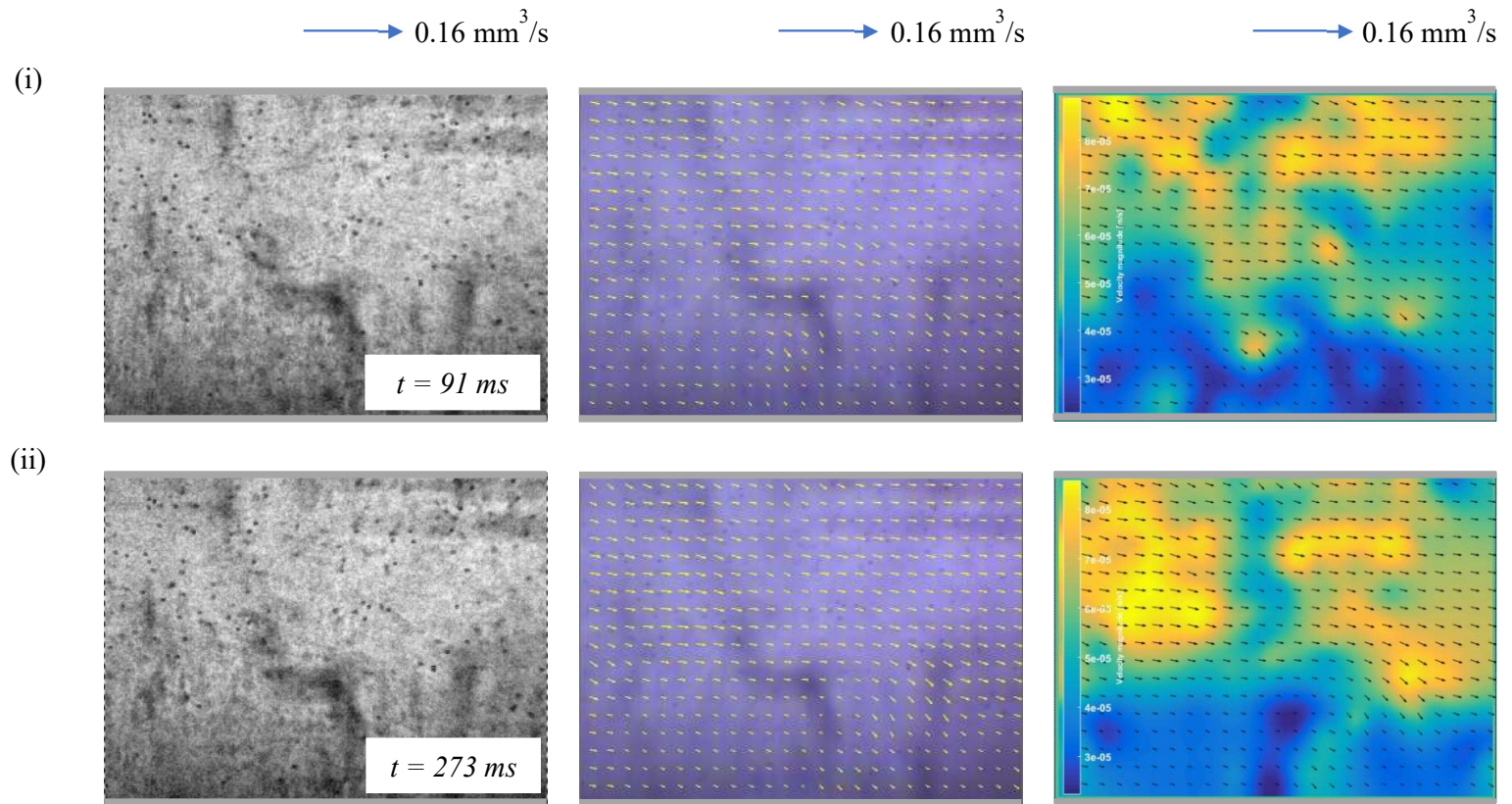
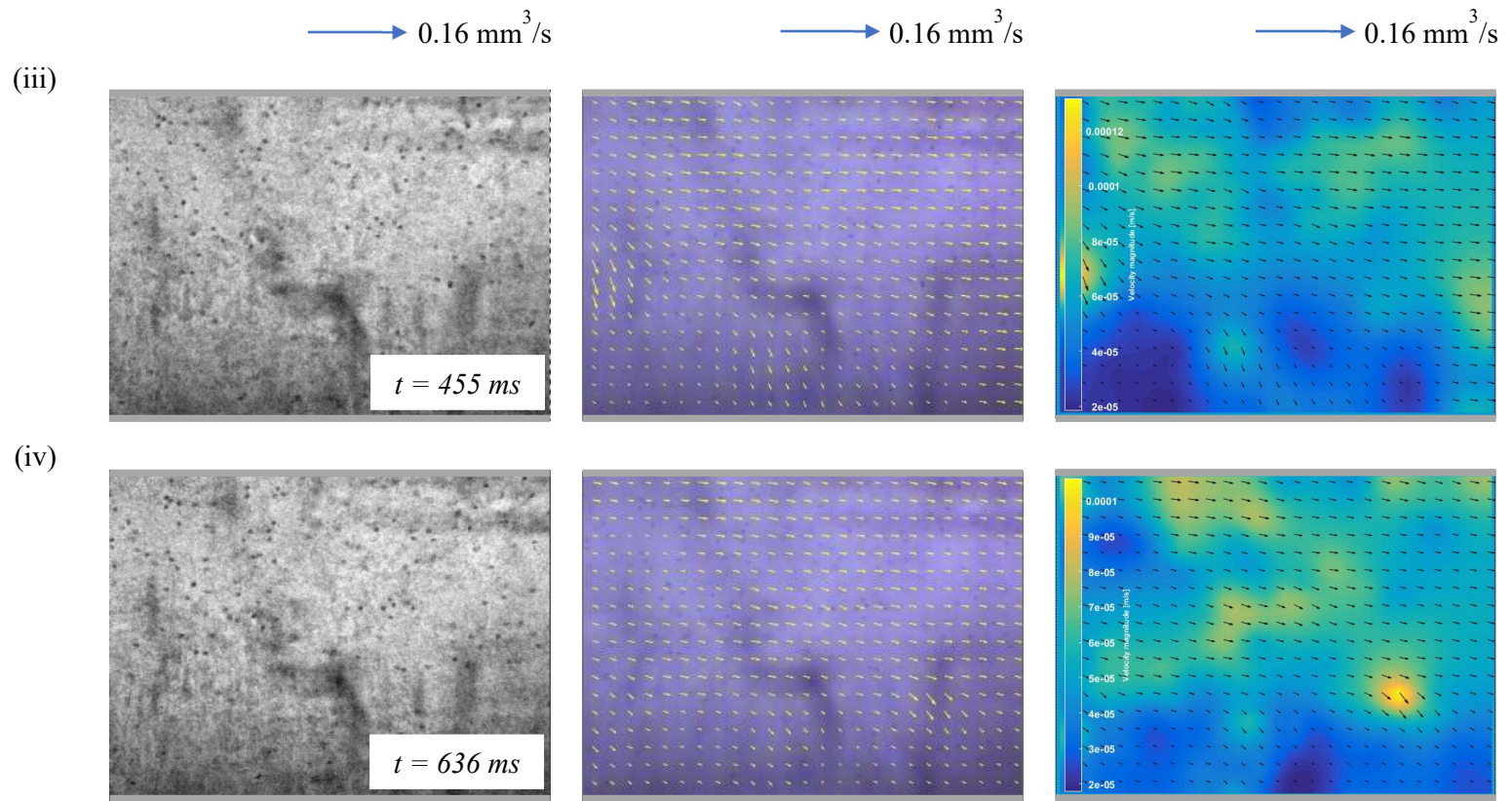


Figure 4.12: Internal velocity profile of generated water droplet for offset T-microchannel with radius of  $750 \mu\text{m}$

(d) radius of 1000  $\mu\text{m}$  offset T-microchannel





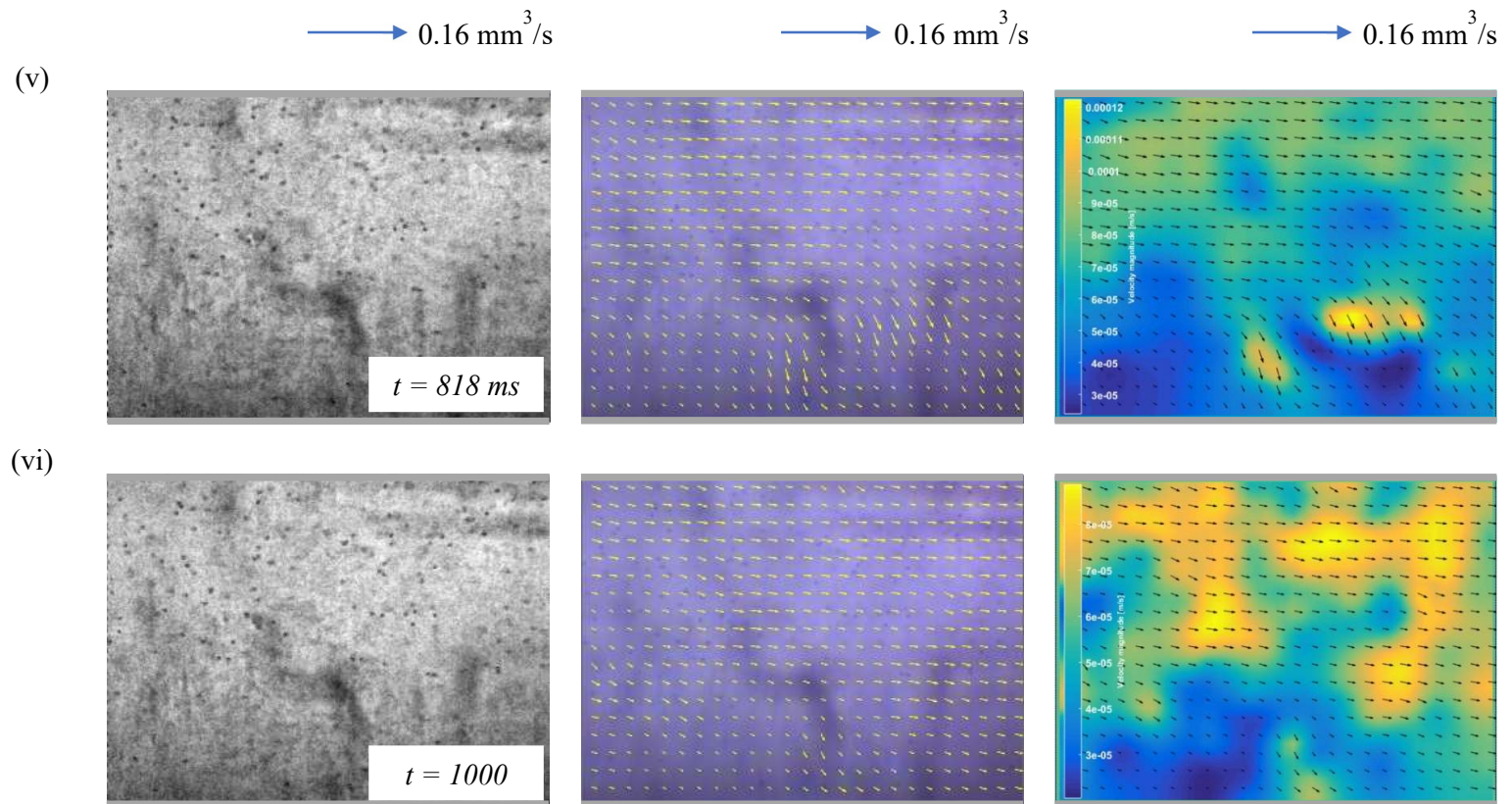


Figure 4.13: Internal velocity profile of generated water droplet for offset T-microchannel with radius of  $1000 \mu\text{m}$

## CHAPTER 5

### CONCLUSION AND RECOMMENDATIONS

#### 5.1 Conclusion

In this research study, micromixing process for three dissimilar liquids which are propan-2-ol, water and sodium chloride solution were experimented in T-junction microchannel at  $5 \leq Re \leq 50$ . Preliminary micromixing experiments showed that it is difficult to characterize immiscible mixture i.e., propan-2-ol and sodium chloride solution due to chaotic mixing at the intersection of T-junction. Hence, in order to smoothly visualize and evaluate their performance, an offset T-junction microchannel was fabricated to overcome this problem. To find the improvement value of mixing performance, the findings for T-junction microchannel was compared with the results for offset T-junction microchannel with same inlet and outlet dimensions. For miscible mixing experiments i.e., propan-2-ol and water, water and sodium chloride solution, both microchannels show that mixing performance of these liquids for each Reynolds number is directly proportional to the mixing time. This is because at low Reynolds number of 5, 10 and 20, the higher residence time allows for higher molecular diffusion as the flow rate is low. Compared to mixing experiment of water and sodium chloride solution in T-junction microchannel, in offset T-junction microchannel, poor mixing of these liquids can be observed at the medium Reynolds number of 30. With increasing Reynolds number from 5 to 30, the mixing performance of these two liquids decreases owing to the enhanced inertial effect with less mixing time from low Reynolds number of 5 to medium Reynolds number of 30. As Reynolds number increases to 40 and 50, under the influence of local vortices and larger inertial force at higher velocity ranging from 0.0030 m/s ( $Re = 5$ ) to 0.0298 m/s ( $Re = 50$ ),

the convection process and mixing quality of propan-2-ol and water, water and sodium chloride solution were improved. As a result, stretching and thinning of liquid lamellae develops dominating convective diffusion compared to molecular diffusion, which influences the mixing process. Besides that, viscosity-density difference also contributed to the increased of mixing index as high viscous and more dense liquid pushed a low viscous and less dense liquid from the channel wall which resulted in an increase of the interface area and consequently improved the mixing in this regime. On the other hand, it is nearly impossible to mix propan-2-ol and sodium chloride solution in the microchannel. In fact, molecular diffusion process between these immiscible liquids is difficult compared to the previous two miscible mixing experiments. Nevertheless, offset T-junction microchannel offers better mixing of propan-2-ol and sodium chloride solution compared to T-junction microchannel at both low and high Reynolds number. Due to the direct collision at the T-junction of the microchannel, chaotic mixing takes place at the intersection at high momentum. When the inlets of T-junction having an offset of 7.5 mm, the mixing quality increases by twice or more.

Due to the fact that offset T-junction can give superior performance than T-junction for immiscible mixture, this research work was furthered by studying the behaviours of distilled water droplet formation suspended in food grade palm olein at interfacial surface in offset T-microchannel having radius of 400  $\mu\text{m}$ , 500  $\mu\text{m}$ , 750  $\mu\text{m}$  and 1000  $\mu\text{m}$  by means of micro-PIV software. These different sizes of inlet and outlet radius of microfluidic channels were affecting the flow behaviours of the multiphase liquids, and also generation of the water droplets. The experimental results show that increasing in the radius of offset T-junction microchannel leads to the increase in cross-sectional area and the decrease of distilled water phase's velocity. The microchannel with radius 400  $\mu\text{m}$  has higher distilled water phase's

velocity than the channel with radius 750  $\mu\text{m}$ . Besides that, the experimental velocity of the distilled water phase's holds a good agreement with theoretical values i.e., radius of 400  $\mu\text{m}$ , 500  $\mu\text{m}$  and 750  $\mu\text{m}$  microchannels have a minimal difference of 0.008 mm/s, 0.06 mm/s and 0.004 mm/s, respectively. For radius of offset T-junction microchannel = 1000  $\mu\text{m}$ , the experimental velocity could not be determined due to the droplet was forming outside the field of view as the image was maintain captured at the junction. The size of the droplets is getting bigger as the radius of microchannel increases and they are nearly equal to the microchannel's width. The channel's radius of 400  $\mu\text{m}$ , 500  $\mu\text{m}$ , 750  $\mu\text{m}$  and 1000  $\mu\text{m}$ , respectively has average velocity of 0.25 mm/s, 0.15 mm/s, 0.055 mm/s and 0.055 mm/s at  $t = 91$  ms. As they reached  $t = 1000$  ms, the average velocity of channel with radius of 400  $\mu\text{m}$  decreased slightly to 0.12 mm/s which might due to the roughness on the channel's surface, while the other channels showed a good and maintained average velocity data i.e., 0.2 mm/s for channel radius of 500  $\mu\text{m}$ , 0.15 mm/s for channel with radius of 750  $\mu\text{m}$ , and 0.055 m/s for channel with radius of 1000  $\mu\text{m}$ . This concludes that the vector and velocity magnitude data in a good agreement with Hagen-Poiseuille flow equation, meaning that a small increase in the channel's internal diameter yields a significant increase in overall flow of a liquid.

## **5.2 Recommendations**

The characterization of mixing index and the droplet generation requires some improvement, especially in terms of the microscope's working principle/ability as it is believably influencing the overall performance of the system. The recommendations are as follow:

(a) Higher power objective lens i.e., 20× magnification as it can provide a higher degree of magnification, which allows to zoom in closer to the sample being studied and see it in more detail.

(b) Higher frame rate, so that smoother and slower the slow motion of fluid flow as the number of frames captured per second increase while maintaining its resolution to produce even more higher quality images.

## REFERENCES

- Ansari, M., Kim, K.-Y., & Kim, S. M. (2010). Numerical study of the effect on mixing of the position of fluid stream interfaces in a rectangular microchannel. *Microsystem technologies*, *16*(10), 1757-1763.
- Ansari, M. A., Kim, K.-Y., & Kim, S. M. (2018). Numerical and experimental study on mixing performances of simple and vortex micro T-mixers. *Micromachines*, *9*(5), 204.
- Ashrafizadeh, S., & Kamran, M. (2010). Emulsification of heavy crude oil in water for pipeline transportation. *Journal of Petroleum Science and Engineering*, *71*(3-4), 205-211.
- Aubin, J., Ferrando, M., & Jiricny, V. (2010). Current methods for characterising mixing and flow in microchannels. *Chemical Engineering Science*, *65*(6), 2065-2093.
- Campo-Deaño, L. (2018). Fluid-flow characterization in microfluidics *Complex Fluid-Flows in Microfluidics* (pp. 53-71): Springer.
- Carcoana, A. (1992). Applied enhanced oil recovery.
- Chen, C.-H., Shah, R. K., Abate, A. R., & Weitz, D. A. (2009). Janus particles templated from double emulsion droplets generated using microfluidics. *Langmuir*, *25*(8), 4320-4323.
- Chen, X., Li, T., Zeng, H., Hu, Z., & Fu, B. (2016). Numerical and experimental investigation on micromixers with serpentine microchannels. *International Journal of Heat and Mass Transfer*, *98*, 131-140.
- Chung, C.-K., & Shih, T. (2008). Effect of geometry on fluid mixing of the rhombic micromixers. *Microfluidics and Nanofluidics*, *4*(5), 419-425.

- Colucci, G., Santamaria-Echart, A., Silva, S. C., Fernandes, I. P., Sipoli, C. C., & Barreiro, M. F. (2020). Development of Water-in-Oil Emulsions as Delivery Vehicles and Testing with a Natural Antimicrobial Extract. *Molecules*, 25(9), 2105.
- Dambrine, J., Geraud, B., & Salmon, J. (2009). Interdiffusion of liquids of different viscosities in a microchannel. *New Journal of Physics*, 11(7), 075015.
- Darekar, M., Singh, K. K., Mukhopadhyay, S., & Shenoy, K. T. (2017). Liquid–liquid two-phase flow patterns in Y-junction microchannels. *Industrial & Engineering Chemistry Research*, 56(42), 12215-12226.
- Deng, C., Huang, W., Wang, H., Cheng, S., He, X., & Xu, B. (2018). Preparation of Micron-Sized Droplets and Their Hydrodynamic Behavior in Quiescent Water. *Brazilian Journal of Chemical Engineering*, 35(2), 709-720.
- Dundi, M., VRK, R., & VP, C. (2019). Characterization of enhanced liquid mixing in T-T mixer at various Reynolds numbers. *Asia-Pacific Journal of Chemical Engineering*, 14(2), e2298.
- Fang, C., Wu, H., Lee, S.-Y., Mahajan, R. L., & Qiao, R. (2018). The ionized graphene oxide membranes for water-ethanol separation. *Carbon*, 136, 262-269.
- Fornerod, M. J., Amstad, E., & Guldin, S. (2020). Microfluidics of binary liquid mixtures with temperature-dependent miscibility. *Molecular Systems Design & Engineering*.
- Fournier, M.-C., Falk, L., & Villiermaux, J. (1996). A new parallel competing reaction system for assessing micromixing efficiency—experimental approach. *Chemical Engineering Science*, 51(22), 5053-5064.
- Fu, H., Liu, X., & Li, S. (2017). Mixing indexes considering the combination of mean and dispersion information from intensity images for the performance estimation of micromixing. *RSC advances*, 7(18), 10906-10914.

- Fu, T., Ma, Y., Funfschilling, D., & Li, H. Z. (2009). Bubble formation and breakup mechanism in a microfluidic flow-focusing device. *Chemical Engineering Science*, *64*(10), 2392-2400.
- Gelin, P., Bihi, I., Ziemecka, I., Thienpont, B., Christiaens, J., Hellemans, K., . . . De Malsche, W. (2020). Microfluidic device for high-throughput production of monodisperse droplets. *Industrial & Engineering Chemistry Research*, *59*(28), 12784-12791.
- Ghannam, M. T. (2003). Emulsion flow behavior of crude oil-Alcoflood polymers. *Journal of Chemical Engineering of Japan*, *36*(1), 35-44.
- Ghannam, M. T. (2005). Water-in-crude oil emulsion stability investigation. *Petroleum Science and Technology*, *23*(5-6), 649-667.
- Giasuddin, H. M., Sanjayan, J. G., & Ranjith, P. (2013). Strength of geopolymer cured in saline water in ambient conditions. *Fuel*, *107*, 34-39.
- Günther, A., Jhunjhunwala, M., Thalmann, M., Schmidt, M. A., & Jensen, K. F. (2005). Micromixing of miscible liquids in segmented gas-liquid flow. *Langmuir*, *21*(4), 1547-1555.
- Hagsäter, S. M., Jensen, T. G., Bruus, H., & Kutter, J. P. (2007). Acoustic resonances in microfluidic chips: full-image micro-PIV experiments and numerical simulations. *Lab on a Chip*, *7*(10), 1336-1344.
- Hein, M., Moskopp, M., & Seemann, R. (2015). Flow field induced particle accumulation inside droplets in rectangular channels. *Lab on a Chip*, *15*(13), 2879-2886.
- Heydari, R., & Mousavi, M. (2016). Simultaneous determination of saccharine, caffeine, salicylic acid and benzoic acid in different matrixes by salt and air-assisted

- homogeneous liquid-liquid extraction and high-performance liquid chromatography. *Journal of the Chilean Chemical Society*, 61(3), 3090-3094.
- Idris, C. A. C., Sundram, K., & Razis, A. F. A. (2018). Effect of Consumption Heated Oils with or without Dietary Cholesterol on the Development of Atherosclerosis. *Nutrients*, 10(10), 1527.
- Jakiela, S., Korczyk, P. M., Makulska, S., Cybulski, O., & Garstecki, P. (2012). Discontinuous transition in a laminar fluid flow: a change of flow topology inside a droplet moving in a micron-size channel. *Physical Review Letters*, 108(13), 134501.
- Jeon, M. K., Kim, J.-H., Noh, J., Kim, S. H., Park, H. G., & Woo, S. I. (2004). Design and characterization of a passive recycle micromixer. *Journal of Micromechanics and Microengineering*, 15(2), 346.
- Jin, B.-J., & Yoo, J. Y. (2012). Visualization of droplet merging in microchannels using micro-PIV. *Experiments in Fluids*, 52(1), 235-245.
- Joensson, H. N., & Andersson Svahn, H. (2012). Droplet microfluidics—A tool for single-cell analysis. *Angewandte Chemie International Edition*, 51(49), 12176-12192.
- Kashid, M. N., & Agar, D. W. (2007). Hydrodynamics of liquid–liquid slug flow capillary microreactor: flow regimes, slug size and pressure drop. *Chemical Engineering Journal*, 131(1-3), 1-13.
- Kim, C.-K., & Yoon, J.-Y. (2017). Optimal design of groove shape on passive micromixer using design of experiment technique. *Proceedings of the Institution of Mechanical Engineers, Part E: Journal of Process Mechanical Engineering*, 231(4), 880-887.
- Kim, M. J., & Breuer, K. S. (2007). Use of bacterial carpets to enhance mixing in microfluidic systems. *Journal of Fluids Engineering*, 129(3), 319-324.

- Kinoshita, H., Kaneda, S., Fujii, T., & Oshima, M. (2007). Three-dimensional measurement and visualization of internal flow of a moving droplet using confocal micro-PIV. *Lab on a Chip*, 7(3), 338-346.
- Kumar Mondal, P., & Wongwises, S. (2020). Magneto-hydrodynamic (MHD) micropump of nanofluids in a rotating microchannel under electrical double-layer effect. *Proceedings of the Institution of Mechanical Engineers, Part E: Journal of Process Mechanical Engineering*, 234(4), 318-330.
- Kuntaegowdanahalli, S. S., Bhagat, A. A. S., Kumar, G., & Papautsky, I. (2009). Inertial microfluidics for continuous particle separation in spiral microchannels. *Lab on a Chip*, 9(20), 2973-2980.
- Lee, C.-Y., Chang, C.-L., Wang, Y.-N., & Fu, L.-M. (2011). Microfluidic mixing: a review. *International Journal of Molecular Sciences*, 12(5), 3263-3287.
- Lee, C.-Y., & Fu, L.-M. (2018). Recent advances and applications of micromixers. *Sensors and Actuators B: Chemical*, 259, 677-702.
- Li, C., Boban, M., & Tuteja, A. (2017). Open-channel, water-in-oil emulsification in paper-based microfluidic devices. *Lab on a Chip*, 17(8), 1436-1441.
- Li, H., Liu, H., Fang, J., Yin, S., Chen, C., & Li, C. (2019). Isopropanol, n-butanol and ethanol recovery from IBE model solutions by salting-out using potassium pyrophosphate. *Journal of Chemical Technology and Biotechnology*, 94(12), 3850-3858.
- Lin, Y.-C., Chung, Y.-C., & Wu, C.-Y. (2007). Mixing enhancement of the passive microfluidic mixer with J-shaped baffles in the tee channel. *Biomedical Microdevices*, 9(2), 215-221.

- Lin, Y., Yu, X., Wang, Z., Tu, S.-T., & Wang, Z. (2011). Design and evaluation of an easily fabricated micromixer with three-dimensional periodic perturbation. *Chemical Engineering Journal*, 171(1), 291-300.
- Liu, Z.-M., & Pang, Y. (2015). Effect of the size and pressure on the modified viscosity of water in microchannels. *Acta Mechanica Sinica*, 31(1), 45-52.
- Liu, Z., Li, M., Pang, Y., Zhang, L., Ren, Y., & Wang, J. (2019). Flow characteristics inside droplets moving in a curved microchannel with rectangular section. *Physics of Fluids*, 31(2), 022004.
- Liu, Z., Zhang, L., Pang, Y., Wang, X., & Li, M. (2017). Micro-PIV investigation of the internal flow transitions inside droplets traveling in a rectangular microchannel. *Microfluidics and Nanofluidics*, 21(12), 180.
- Lobasov, A., Minakov, A., & Rudyak, V. Y. (2016). Viscosity effect on the flow patterns in T-type micromixers. *Fluid Dynamics*, 51(3), 381-388.
- Ma, S., Sherwood, J. M., Huck, W. T., & Balabani, S. (2014). On the flow topology inside droplets moving in rectangular microchannels. *Lab on a Chip*, 14(18), 3611-3620.
- Ma, S., Sherwood, J. M., Huck, W. T., & Balabani, S. (2015). The microenvironment of double emulsions in rectangular microchannels. *Lab on a Chip*, 15(10), 2327-2334.
- Mahmud, F., & Tamrin, K. F. (2020). Method for determining mixing index in microfluidics by RGB color model. *Asia-Pacific Journal of Chemical Engineering*, e2407.
- Mondal, B., Pati, S., & Patowari, P. K. (2020). Numerical Analysis of Mixing Performance in Microchannel with Different Ratio of Outlet to Inlet Width *Techno-Societal 2018* (pp. 257-266): Springer.

- Nagata, M. (2018). Usefulness of underwater endoscopic submucosal dissection in saline solution with a monopolar knife for colorectal tumors (with videos). *Gastrointestinal Endoscopy*, 87(5), 1345-1353.
- Oishi, M., Kinoshita, H., Fujii, T., & Oshima, M. (2011). Simultaneous measurement of internal and surrounding flows of a moving droplet using multicolour confocal micro-particle image velocimetry (micro-PIV). *Measurement Science and Technology*, 22(10), 105401.
- Omori, T., Imai, Y., Kikuchi, K., Ishikawa, T., & Yamaguchi, T. (2015). Hemodynamics in the microcirculation and in microfluidics. *Annals of Biomedical Engineering*, 43(1), 238-257.
- Ooms, T., Lindken, R., & Westerweel, J. (2009). Digital holographic microscopy applied to measurement of a flow in a T-shaped micromixer. *Experiments in Fluids*, 47(6), 941.
- Orsi, G., Roudgar, M., Brunazzi, E., Galletti, C., & Mauri, R. (2013). Water–ethanol mixing in T-shaped microdevices. *Chemical Engineering Science*, 95, 174-183.
- Pang, L., Shen, S., Ma, C., Ma, T., Zhang, R., Tian, C., . . . Wang, J. (2015). Deformability and size-based cancer cell separation using an integrated microfluidic device. *Analyst*, 140(21), 7335-7346.
- Pang, Y., Kim, H., Liu, Z., & Stone, H. A. (2014). A soft microchannel decreases polydispersity of droplet generation. *Lab on a Chip*, 14(20), 4029-4034.
- Salim, A., Fourar, M., Pironon, J., & Sausse, J. (2008). Oil–water two-phase flow in microchannels: Flow patterns and pressure drop measurements. *The Canadian Journal of Chemical Engineering*, 86(6), 978-988.
- Santiago, J. G., Wereley, S. T., Meinhart, C. D., Beebe, D., & Adrian, R. J. (1998). A particle image velocimetry system for microfluidics. *Experiments in Fluids*, 25(4), 316-319.

- Shah, I., Kim, S. W., Kim, K., Doh, Y. H., & Choi, K. H. (2019). Experimental and numerical analysis of Y-shaped split and recombination micro-mixer with different mixing units. *Chemical Engineering Journal*, 358, 691-706.
- Shah, I., Su Jeon, H., Ali, M., Yang, D. H., & Choi, K.-H. (2019). Optimal parametric mixing analysis of active and passive micromixers using Taguchi method. *Proceedings of the Institution of Mechanical Engineers, Part E: Journal of Process Mechanical Engineering*, 233(6), 1292-1303.
- Shah, R., Shum, H., Rowat, A., Lee, D., Agresti, J., & Utada, A. (2008). CL Y., JW Kim, A. Fernandez-Nieves, CJ Martinez and DA Weitz. *Materials Today*, 11, 18-27.
- Shen, F., Li, Y., Liu, Z., & Li, X. (2017). Study of flow behaviors of droplet merging and splitting in microchannels using Micro-PIV measurement. *Microfluidics and Nanofluidics*, 21(4), 66.
- Shinohara, K., Sugii, Y., Aota, A., Hibara, A., Tokeshi, M., Kitamori, T., & Okamoto, K. (2004). High-speed micro-PIV measurements of transient flow in microfluidic devices. *Measurement Science and Technology*, 15(10), 1965.
- Siddique, B. M., Ahmad, A., Ibrahim, M. H., Hena, S., & Rafatullah, M. (2010). Physico-chemical properties of blends of palm olein with other vegetable oils. *Grasas y Aceites*, 61(4), 423-429.
- Sjöblom, J. (2012). *Emulsions: a fundamental and practical approach* (Vol. 363): Springer Science & Business Media.
- Solehati, N., Bae, J., & Sasmito, A. P. (2014). Numerical investigation of mixing performance in microchannel T-junction with wavy structure. *Computers & Fluids*, 96, 10-19.

- Teh, S.-Y., Lin, R., Hung, L.-H., & Lee, A. P. (2008). Droplet microfluidics. *Lab on a Chip*, 8(2), 198-220.
- Thielicke, W. (2014). The flapping flight of birds. *Diss. University of Groningen*.
- Thielicke, W., & Stamhuis, E. (2014). PIVlab—towards user-friendly, affordable and accurate digital particle image velocimetry in MATLAB. *Journal of open research software*, 2(1).
- Thurgood, P., Baratchi, S., Arash, A., Pirogova, E., Jex, A. R., & Khoshmanesh, K. (2019). Asynchronous generation of oil droplets using a microfluidic flow focusing system. *Scientific Reports*, 9(1), 1-11.
- Turner, A., Yandrofski, K., Telikepalli, S., King, J., Heckert, A., Filliben, J., . . . Schiel, J. E. (2018). Development of orthogonal NISTmAb size heterogeneity control methods. *Analytical and Bioanalytical Chemistry*, 410(8), 2095-2110.
- Viktorov, V., Mahmud, M. R., & Visconte, C. (2016). Numerical study of fluid mixing at different inlet flow-rate ratios in Tear-drop and Chain micromixers compared to a new HC passive micromixer. *Engineering Applications of Computational Fluid Mechanics*, 10(1), 182-192.
- Vladislavljević, G. T., Al Nuamani, R., & Nabavi, S. A. (2017). Microfluidic production of multiple emulsions. *Micromachines*, 8(3), 75.
- Vuckovac, M., Backholm, M., Timonen, J. V., & Ras, R. H. (2020). Viscosity-enhanced droplet motion in sealed superhydrophobic capillaries. *Science advances*, 6(42), eaba5197.
- Wang, H., Iovenitti, P., Harvey, E., & Masood, S. (2002). Optimizing layout of obstacles for enhanced mixing in microchannels. *Smart Materials and Structures*, 11(5), 662.

- Wang, J., Wang, J., Feng, L., & Lin, T. (2015). Fluid mixing in droplet-based microfluidics with a serpentine microchannel. *RSC advances*, 5(126), 104138-104144.
- Wang, S., Huang, X., & Yang, C. (2011). Mixing enhancement for high viscous fluids in a microfluidic chamber. *Lab on a Chip*, 11(12), 2081-2087.
- Wang, W., Zhao, S., Shao, T., Jin, Y., & Cheng, Y. (2012). Visualization of micro-scale mixing in miscible liquids using  $\mu$ -LIF technique and drug nano-particle preparation in T-shaped micro-channels. *Chemical Engineering Journal*, 192, 252-261.
- Wang, X., Liu, G., Wang, K., & Luo, G. (2015). Measurement of internal flow field during droplet formation process accompanied with mass transfer. *Microfluidics and Nanofluidics*, 19(3), 757-766.
- Wu, B., von der Ecken, S., Swyer, I., Li, C., Jenne, A., Vincent, F., . . . Busse, F. (2019). Rapid Chemical Reaction Monitoring by Digital Microfluidics-NMR: Proof of Principle Towards an Automated Synthetic Discovery Platform. *Angewandte Chemie International Edition*, 58(43), 15372-15376.
- Wu, Y.-A., Panigrahi, B., Lu, Y.-H., & Chen, C.-Y. (2017). An integrated artificial cilia based microfluidic device for micropumping and micromixing applications. *Micromachines*, 8(9), 260.
- Xie, S., Yi, C., & Qiu, X. (2016). Salting-out effect of potassium pyrophosphate (K<sub>4</sub>P<sub>2</sub>O<sub>7</sub>) on the separation of biobutanol from an aqueous solution. *Journal of Chemical Technology and Biotechnology*, 91(6), 1860-1867.
- Xu, B.-B., Ma, Z.-C., Wang, L., Zhang, R., Niu, L.-G., Yang, Z., . . . Xu, Y. (2011). Localized flexible integration of high-efficiency surface enhanced Raman scattering (SERS) monitors into microfluidic channels. *Lab on a Chip*, 11(19), 3347-3351.

- Yao, J., Lin, F., Kim, H. S., & Park, J. (2019). The effect of oil viscosity on droplet generation rate and droplet size in a T-junction microfluidic droplet generator. *Micromachines*, *10*(12), 808.
- Zhang, J.-w., Liu, S.-f., Cheng, C., Li, W.-f., Xu, X.-l., Liu, H.-f., & Wang, F.-c. (2019). Investigation of three-dimensional flow regime and mixing characteristic in T-jet reactor. *Chemical Engineering Journal*, *358*, 1561-1573.
- Zhu, P., Tang, X., & Wang, L. (2016). Droplet generation in co-flow microfluidic channels with vibration. *Microfluidics and Nanofluidics*, *20*(3), 47.
- Zhu, Q., Pan, Y., Jia, X., Li, J., Zhang, M., & Yin, L. (2019). Review on the stability mechanism and application of water-in-oil emulsions encapsulating various additives. *Comprehensive Reviews in Food Science and Food Safety*, *18*(6), 1660-1675.

## **APPENDICES**

### **Journal Publications**